THE JOURNAL OF PHYSICAL CHEMISTRY B

Feature Article

pubs.acs.org/JPCB

Proteins at Interfaces Probed by Chiral Vibrational Sum Frequency Generation Spectroscopy

Elsa C. Y. Yan,* Zhuguang Wang, and Li Fu†

Department of Chemistry, Yale University, New Haven, CT 06511, United States

ABSTRACT: Characterizations of protein structures at interfaces are important in solving an array of fundamental and engineering problems, including understanding transmembrane signal transduction and molecular transport processes and development of biomaterials to meet the needs of biomedical and energy research. However, in situ and real-time characterization of protein secondary structures is challenging because it requires physical methods that are selective to both interface and secondary structures. Here, we summarize recent experimental developments in our laboratory of chiral vibrational sum frequency generation spectroscopy (SFG) for analyzing protein structures at interfaces. We showed that chiral SFG provides vibrational optical signatures of the peptide N−H stretch and amide I modes that can distinguish various protein secondary structures. Using these signatures, we further applied chiral SFG to probe orientations and folding kinetics of proteins at interfaces. Our results show that chiral SFG is a background-free, label-free, in situ, and real-time vibrational method for studying proteins at interfaces. This recent progress demonstrates the potential of chiral SFG in solving problems related to proteins and other chiral biopolymers at interfaces.

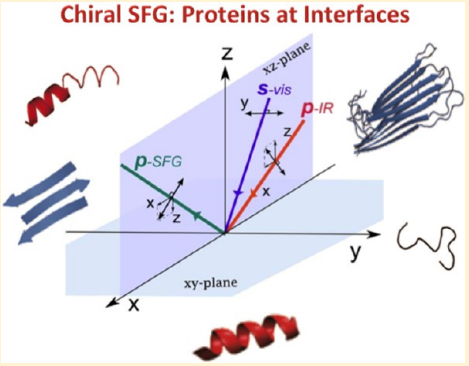

1. INTRODUCTION

Quantitative structural and orientation analyses of proteins at interfaces are important because they are related to an array of fundamental and engineering problems (Figure 1). Examples include biological processes mediated by protein−membrane interactions, such as molecular transport across cell membrane,[1,2] adhesion of cells,[3] immunological response, and signal transduction across the cell membrane.[4] Aside from these biological processes, biomedical applications also require knowledge of protein structures at interfaces (e.g., drug delivery and biosensors). Added to these applications are the needs of new materials in biomedical research and energy research,[5] such as smart materials, organic/inorganic hybrid, heterogeneous biocatalysts, etc. Thus, protein characterization at the interface can aid fundamental understanding of the biological processes and development of new materials and molecular devices.

Proteins are biopolymer made with 20 amino acids. The sequence of amino acids, translated from a genetic sequence, determines the fold and structure of each protein, which, in turn, enables the designated biological functions. In general, native proteins with molecular weights ranging from a few to over thousands of kD (Scheme 1) can fold into various domains. Although the folded protein structures can be complex (Scheme 1), they can be dissected into various secondary structures, such as parallel β-sheet, antiparallel β-sheet, α-helix, 3_{10}-helix, and disordered structures. These secondary structures are the basic building blocks and functional units of proteins. Thus, knowledge about secondary structures of proteins is fundamental to the understanding of the molecular mechanism and functions of the proteins.

Although characterization methods for protein secondary structures in aqueous solution has been available for decades, such as NMR and circular dichroism, knowledge about secondary structures of any particular protein in aqueous solution cannot be directly extrapolated to interfaces. This is because interfaces have environments drastically different from bulk phases.[6] This argument becomes clear when we consider the air/water interface. Although we know very well the physical properties of both air and water (e.g., dielectric constant, density, refractive index, etc.), these physical properties are still largely unknown at the air/water interface. Hence, structures and functions of proteins at interfaces are expected to be different from those in the bulk aqueous solution. Even though a protein of interest has been extensively characterized in aqueous solution, we cannot assume that it is in the same structure and able to function at the surfaces of cell, biosensors, and heterogeneous biocatalysts, etc. Consequently, it is necessary to observe protein secondary structures at interfaces in situ.

Nonetheless, characterization of protein secondary structures at interfaces is challenging. The challenge comes from the need for physical methods that are selective to both interfaces and secondary structures. Selectivity of the interface means that the methods are sensitive only to molecules at interfaces but not in bulk solution, such that information about interfaces will not be masked by the bulk signals. Also, the methods should be muted to water solvent; otherwise, water background will overwhelm the signals generated by proteins at interfaces. In addition, the

Received: September 3, 2014
Revised: November 26, 2014
Published: January 7, 2015

DOI: 10.1021/jp508926e
J. Phys. Chem. B 2015, 119, 2769−2785

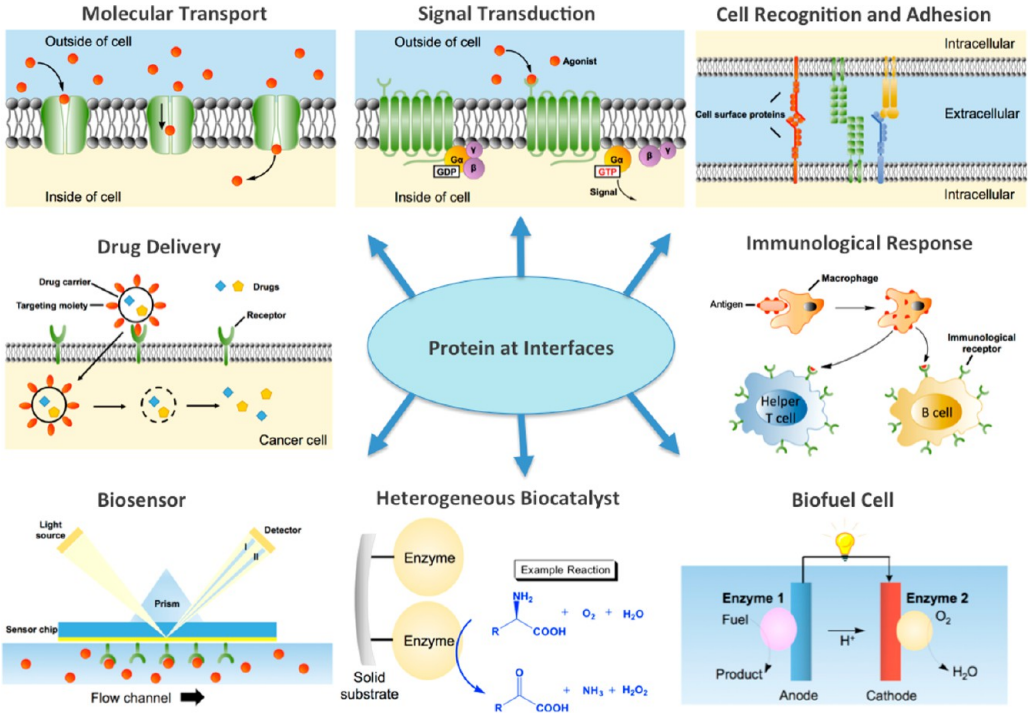

Figure 1. Fundamental and engineering problems related to proteins at interfaces: molecular transport across cell membranes, transmembrane signal transduction, cell recognition and adhesion, drug delivery across cell membranes, immunological responses, biosensor, heterogeneous biocatalysts, and enzymes on electrodes of biofuel cells.

Scheme 1. Prototypical Proteins Containing Various Domains and Secondary Structures: α-Helix (Red), Antiparallel β-Sheet (Yellow), Parallel β-Sheet (Blue), 3_{10}-Helix (Magenta), and Disordered Structures (Grey)

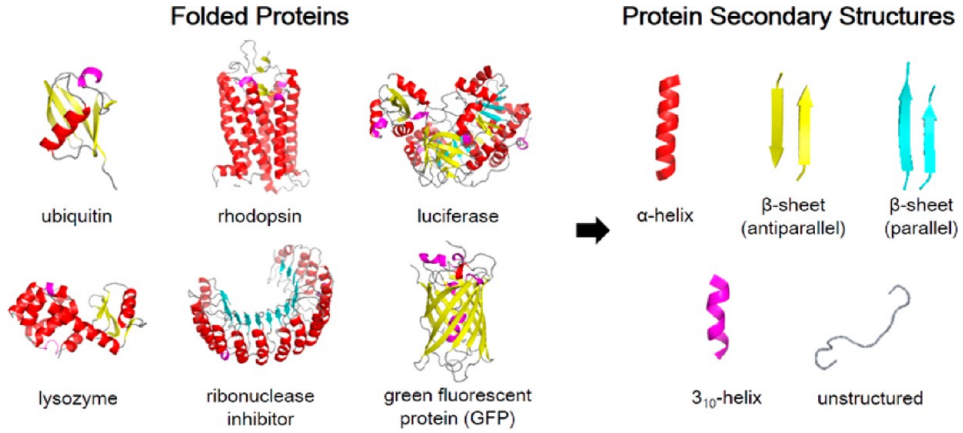

physical methods need to provide signals that are characteristic of protein secondary structures. Circular dichroism,[7] NMR,[8−11] and more recently two-dimensional (2D) infrared spectroscopy[12−18] allow characterizations of protein secondary structures. However, these methods are not surface-selective. Infrared reflectance absorption spectroscopy (IRRAS) detects absorption of an infrared (IR) beam reflected from an interface.[19,20] Since the signal is reflected from an interface, it carries surface information. Protein characterization using IRRAS[21−23] relies on the amide I vibrational mode (a combination of peptide C═O stretch, N−C stretch, and N−H bending modes) characteristic of various protein secondary structures (Table 1).[24−29] The IR amide I bands have been successfully used to resolve β-sheet structures from disordered structures and α-helical structures because the amide I bands of β-sheets are at relatively low (<1640 cm^{-1}) and high (>1660 cm^{-1}) characteristic frequencies.[24−29]

Table 1. Amide I Frequencies Characteristic of Protein Secondary Structures, Summary of Results Reported in Refs 24−29

	band position in H_2O (cm^{-1})	
secondary structure	average	extremes
α-helix	1654	1648−1660
antiparallel and parallel β-sheet	1633	1612−1641
antiparallel β-sheet	1684	1674−1695
turns	1672	1660−1686
disordered	1654	1640−1660

However, resolving disordered structures and α-helical structures can potentially be ambiguous as their amide I bands overlap (Table 1). Moreover, water's O−H bending mode at ~1600 cm^{-1} overlaps with the amide I region; thus, D_2O is needed to

DOI: 10.1021/jp508926e
J. Phys. Chem. B 2015, 119, 2769−2785

reduce the background. Since hydrogen bonds are stronger involving deuterium, possible perturbations to protein structures and functions need to be considered. Apart from IRRAS, achiral (conventional) vibrational sum frequency generation (SFG) spectroscopy has been used to probe protein structures at interfaces. The studies mostly focus on characterization of amide I bands[30−38] and thus suffer from the same challenge of spectral deconvolution. Therefore, we need a new physical method complementary to current techniques for characterizing protein secondary structures at interfaces.

Here, we present our work reported in the past five years on developing chiral vibrational SFG spectroscopy for characterization of protein secondary structures at interfaces, which is built on the pioneers' work in the field of nonlinear surface spectroscopy, including Shen who first detected chiral vibrational SFG signals from bulk solution,[39−42] Simpson who formulated chiral SFG theory to explain the surface selectivity of the method,[43,44] Wang who derived quantitative description of chiral second-order optical signals,[45] Chen who performed the first experiments to detect surface-specific chiral SFG amide I signal from protein,[46] and Geiger who extended the chiral vibrational SFG method to study chirality of double-helix DNA molecules on solid substrates.[47,48] On the basis of these studies, we expanded protein characterizations at interfaces using chiral SFG from the use of amide I vibrational modes to the use of N−H stretch modes and systematically characterized the peptide N−H stretch and amide I of a series of model protein systems in various secondary structures.[49−54] In performing these experiments, we identified a set of chiral vibrational signatures for various protein secondary structures at interfaces. Using these signatures, we probed structures,[49,51,52] orientation,[54] folding,[49−51] and proton exchange[53] of proteins at interfaces. This review summarizes these results, which demonstrate the promise of chiral vibrational SFG as a new vibrational method for studying proteins at interfaces in situ and in real time with selectivity to both interfaces and protein secondary structures.

Below, we will first provide a brief description of chiral vibrational SFG theory[43,44,55] and then describe the applications of chiral SFG in the studies of amyloid aggregation at lipid/water interfaces,[49−51] followed by a presentation of amide I and H−N stretch chiral SFG spectra of a series of model peptides and proteins.[49,51] We will then show the applications of chiral SFG in probing kinetics and structures of proteins at interfaces.[53,54,56] Finally, we will discuss the outlooks of the method in addressing various fundamental and engineering problems and identify the challenges, where physical chemists can contribute to further development of the method into a quantitative approach for solving problems in various fields ranging from biomedical science and material science to energy research.

2. BASIC PRINCIPLE OF CHIRAL VIBRATIONAL SFG

Sum frequency generation spectroscopy is a second-order optical method. It is surface-specific due to the noncentrosymmetric properties of interfaces under the dipole approximation.[45,57−62] Because of the asymmetric forces that act on molecules at interfaces, molecules at interfaces are aligned. Thus, interfaces are anisotropic, as exemplified by a long-chain alcohol at the air/water interface (Scheme 2).[63] In bulk media, asymmetric forces are absent; thus, molecules are randomly oriented. When two laser beams overlap spatially and temporally at the interface, the second order polarization induced at the aligned molecules can generate the SFG electric field that can add up coherently, leading to SFG signals (Scheme 2). However, the second-order

Scheme 2. Noncentrosymmetric Interface versus a Centrosymmetry Bulk Medium

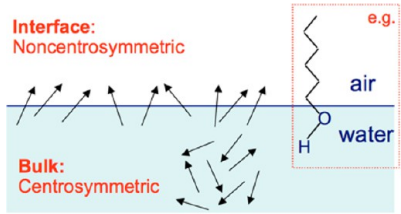

polarization induced at the randomly oriented molecules in bulk media cancel, resulting in no SFG signal. Thus, second-order SFG spectroscopy is surface-specific.

The SFG method is sensitive to vibrational structures at interfaces. In an SFG experiment, two laser beams are used: one in the mid-infrared frequency (ω_{IR}) and one in the visible

Scheme 3. Second-Order Optical Process of Vibrational SFG Spectroscopy

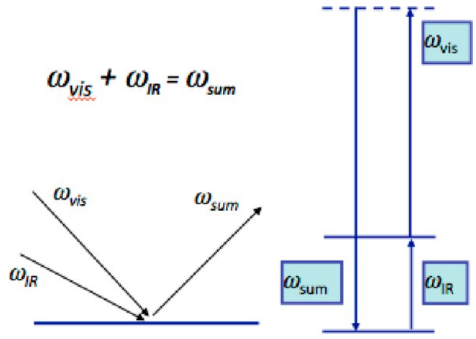

frequency (ω_{vis}) (Scheme 3). The SFG signals generated at frequency ($\omega_{IR} + \omega_{vis}$) can be described as

$$I_{SFG} \propto \left| \chi^{(2)}_{NR} + \sum_q \frac{A_q}{\omega_{IR} - \omega_q + i\Gamma} \right|^2 \quad (1)$$

where I_{SFG} is the SFG intensity, $\chi^{(2)}_{NR}$ is the nonresonant second-order susceptibility, ω_{IR} is the input IR frequency, and A_q, ω_q, and Γ_q are the amplitude, resonant frequency, and damping factor of the qth vibration mode, respectively. In vibrational SFG experiments, the incident visible frequency is often fixed, while the IR frequency is varied. When the IR frequency approaches the vibrational frequency of the qth vibrational mode of the molecules at the interface, the SFG signals can be enhanced due to resonance effects. Therefore, in simple terms, SFG is a surface-specific vibrational spectroscopy.

Then, how can the SFG method be used to probe chiral vibrational structures at interfaces? Here, we confine our discussion under the conditions: (1) the incident visible frequency is not in resonance with electronic transition of the molecular systems under study and (2) a chiral anisotropic interface is in contact with isotropic bulk media. These are the preconditions for surface-specificity of chiral vibrational SFG.[55] Under these conditions, one needs to choose the polarization setting for the incident beams and the SFG signal to selectively probe surface chirality. To explain this, we use the formulation that was first proposed by the Simpson group.[43,44] We consider

DOI: 10.1021/jp508926e
J. Phys. Chem. B 2015, 119, 2769−2785

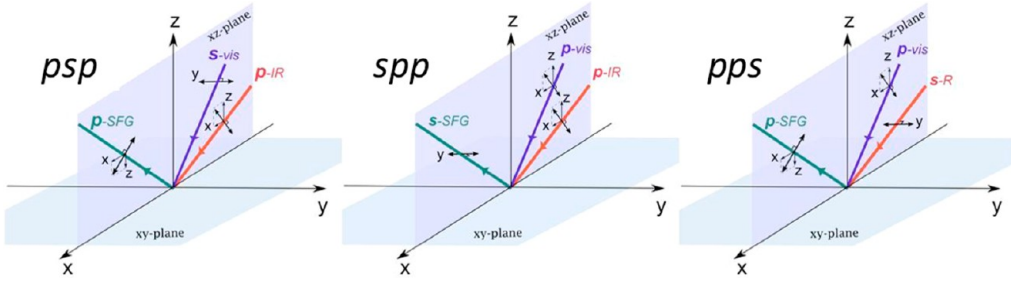

Figure 2. Three polarization settings (*psp*, *spp*, and *pps*) for detection of chiral SFG signals: the *p*- and *s*-polarized beams with their electric field projected onto the laboratory frame (*x*, *y*, *z*). Reprinted from ref 55. Copyright 2014 American Chemical Society.

the measured SFG intensity (I_{SFG}) directly proportional to the square of the optical electric field (E_{SFG}):

$$I_{SFG} = |\vec{E}_{SFG}|^2$$

$$\vec{E}_{SFG} = E^x_{SFG}\hat{x} + E^y_{SFG}\hat{y} + E^z_{SFG}\hat{z} \quad (2)$$

where (*x*, *y*, *z*) are the laboratory coordinates, E^x_{SFG}, E^y_{SFG}, and E^z_{SFG} are the projections of the SFG electric field onto the *x*, *y*, and *z* Cartesian laboratory coordinates, respectively. The SFG electric field is related to the optical electric fields of the incident visible (E^J_{vis}) and IR (E^K_{IR}) beams:

$$E^I_{SFG} \propto \sum_{JK} \chi^{(2)}_{IJK} E^J_{vis} E^K_{IR} \quad (3)$$

where *I*, *J*, and *K* denote the direction of the SFG, visible, and IR fields in the laboratory coordinates (*x*, *y*, *z*), respectively, and $\chi^{(2)}_{IJK}$ is a tensor element in the second-order susceptibility tensor $\chi^{(2)}$.[45] The second-order susceptibility tensor contains all the structural and orientation information about the interface. In SFG experiments, linearly polarized incident beams are often used (Figure 2), either *s*-polarized (electric field perpendicular to the incident *xz* plane) or *p*-polarized (electric field parallel to the incident *xz* plane), and signals are measured using either *s*- or *p*-polarization (Figure 2). Since each beam can be in either *s*- or *p*-polarization, there are a total of (2 × 2 × 2 =) 8 possible polarization settings. These polarizations are denoted as *ppp*, *pps*, *psp*, *pss*, *spp*, *sps*, *ssp*, and *sss*, where the indices indicate the polarization of the beams from high-to-low frequency (i.e., SFG, visible, and then IR). Among these eight settings, three can be used for chiral SFG, including *psp*, *spp*, and *pps* (Figure 2).[43,44,51,55]

Here, we use *psp* as an example to illustrate the basic principle of chiral selectivity.[51,55] For *psp* polarization (Figure 2), the *p*-polarized SFG and IR beams have an electric field projected onto the *x*- and *z*-directions, while the *s*-polarized visible beam has an electric field projected only onto the *y*-direction. Since the first index of $\chi^{(2)}$ tensor elements depicts the electric field of the SFG beam, the second index the visible beam, and the third the IR beam, among the 27 elements in the $\chi^{(2)}$ tensor, only four are relevant: χ_{xyx}, χ_{xyz}, χ_{zyx}, and χ_{zyz}. Among these four tensor elements, χ_{xyx} and χ_{zyz} are zero due to C_∞ symmetry of an isotropic interface (Scheme 4).[55,62] Also, χ_{xyz} is zero in the absence of electronic resonance. This is because the Raman tensor is symmetric, and it follows that the first two indices describing the Raman polarization are exchangeable (i.e., $\chi_{xyz} = \chi_{yxz}$). With C_∞ symmetry of a chiral surface, imposing a C_4 rotation about the surface normal gives $\chi_{xyz} = \chi_{(-y)(x)z} = -\chi_{yxz}$. This, combined with $\chi_{xyz} = \chi_{yxz}$, leads to $\chi_{xyz} = -\chi_{xyz} = 0$. Consequently, χ_{zyx} is the only tensor elements measured by the *psp* polarization. Similar arguments can also be applied to the *spp* and *pps* polarizations, showing that these two settings also measure only χ_{zyx}.[55] Since χ_{zyx} is orthogonal, meaning that $I \neq J \neq K$, χ_{zyx} has inherited handedness similar to the Cartesian coordinates. Thus, only when the surface is chiral will χ_{zyx} be nonzero, yielding chiral specific signals. Therefore, the *psp*, *spp*, and *pps* polarizations can be used to probe surface chirality.

Scheme 4. Symmetry of a Chiral Surface and the Non-Zero Achiral and Chiral Second-Order Susceptibility Tensor Elements

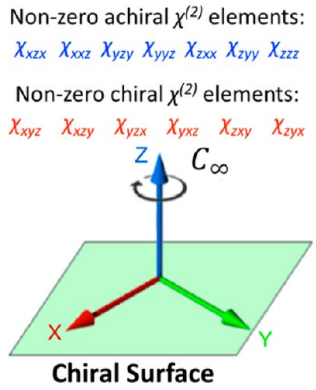

In addition, mixed polarization (*m*) of *s* and *p* is also used to extract chiral information at interfaces. This polarization can introduce achiral contribution to the chiral element of SFG signals. For instance, the effective $\chi^{(2)}$ of *pm+p* and the *pm-p* polarization can be expressed as[42,48,64,65]

$$\chi^{(2)}_{pm\pm p} = \cos(m)\chi^{(2)}_{ppp} \pm \sin(m)\chi^{(2)}_{psp} \quad (4)$$

where *m* is the polarization angle. The intensity difference of the *pm+p* and the *pm-p* spectra can be calculated as

$$I_{pm+p} - I_{pm-p} = 4\cos(m)\sin(m)\,\mathrm{Re}(\chi^{(2)}_{ppp}\chi^{(2)}_{psp}) \quad (5)$$

which includes the interference between the achiral (*ppp*) and the chiral (*psp*) susceptibility terms. If $\chi^{(2)}_{ppp}$ is larger than $\chi^{(2)}_{psp}$, the chiral SFG signal can be enhanced. This interference method has been used to enhance or validate chiral SFG signals that are otherwise difficult to do with direct measurement.[46,52,65,66]

3. APPLICATION OF CHIRAL VIBRATIONAL SFG TO AMYLOID AGGREGATION AT INTERFACES

In our first set of chiral SFG experiments, we used the *psp* polarization setting to study amyloid aggregation at the lipid/water interface.[49−51] Amyloid proteins are important because they are associated with a number of diseases, such as Alzheimer's, Parkinson's, Huntingon's, and prion diseases

DOI: 10.1021/jp508926e
J. Phys. Chem. B 2015, 119, 2769−2785

(Table 2).[67−69] In the normal states, the amyloid proteins are in relatively disordered structures, but in the diseased states, they aggregate into β-sheet rich structures and deposited onto the related tissues. It is important to investigate amyloid aggregation upon interactions with cell membrane for at least two reasons. First, in the past, it was believed that the final aggregation products, the highly ordered fibrils, are cytotoxic. However, in the past decade, increasing numbers of studies have shown that the early aggregation product in small oligomeric forms can interact with the cell membrane,[70−75] disrupting membrane integrity and causing cytotoxicity. Second, lipid membrane has been shown to catalyze the aggregation process, leading to various models for the mechanism.[76−79] For example, Scheme 5 describes an amyloid protein upon interactions with membrane surface folds from disordered structures to α-helical structures and then β-sheets.[22,71] Consequently, it is important to understand the early events of amyloid aggregation on membrane surfaces.

Table 2. Diseases Associated with Amyloid Proteins

diseases	amyloid proteins
Alzheimer's disease	β-amyloid
Parkinson's disease	α-synuclein
Huntington's disease	polyglutamine
Prion disease	prion protein
type II diabetes	islet amyloid polypeptide (IAPP)

Scheme 5. Aggregation of Amyloid Proteins from Disordered Structures to α-Helical and then β-Sheet Structures on a Membrane Surface. Reprinted from ref 49. Copyright 2011 American Chemical Society.

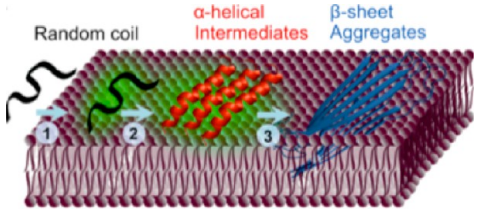

Nonetheless, it is not straightforward to observe amyloid aggregation in early stages on membrane surfaces (Scheme 5) because it requires a physical method that can distinguish protein secondary structures and selectively probe amyloid proteins at interfaces without interference from bulk media, particularly when amyloid proteins also exist in bulk solution often at high concentration in the diseased state. While NMR and circular dichroism can reveal protein secondary structures, the signals are interfered by the contributions of amyloid proteins in bulk solution. Previously, IRRAS was used to probe the protein aggregation process, yielding mechanistic understanding of amyloid aggregation upon interactions with lipid at interfaces.[22] However, deconvolution of the IR spectra into contributions from disordered, α-helical, and β-sheet structures can still be challenging. Here, we applied chiral vibrational SFG together with conventional (achiral) SFG to probe aggregation of human islet amyloid polypeptide (hIAPP) induced by phospholipids at the air/water interface (Scheme 6).

The hIAPP peptide is associated with type II diabetes.[67,69] It is expressed in β cells in the pancreas, containing 37 amino acids (Scheme 6). In the normal state, hIAPP is in relatively disordered structures. In the diseased state, it aggregates into β-sheet-rich amyloid. The aggregation is linked to the death of β cells that produce insulin. Lipid membrane is known to catalyze the aggregation process (Scheme 5).[76−79] Intriguingly, islet amyloid polypeptide is expressed not only in human but also in other mammals, such as rat. Rat islet amyloid polypeptide (rIAPP) is different from hIAPP by 6 amino acids (Scheme 6). Because of these differences, rIAPP does not aggregate and rats do not have type II diabetes.[80] Hence, rIAPP is an ideal control system that aids spectral interpretation in method developments.

To perform the experiments, we used a broad-bandwidth SFG spectrometer (Figure 3), described in detail in Ma et al.[63] The spectrometer provided a 120 fs pulsed IR beam and a 2 ps pulsed visible (800 nm) beam at a repetition rate of 5 kHz. The IR beam is tunable from 900 to 3800 cm^{-1}. The IR and visible beams spatially and temporally overlap at the air/water interface to generate the SFG signals, which were detected by a CCD in reflection geometry.

In the first experiment (Figure 4), we obtained the chiral and achiral SFG spectra in the amide I region from the air/water interface of the IAPP solutions at 1 μM in a phosphate buffer (10 mM, pH 7.4) in the absence and presence of negatively charged phospholipid,[50] dipalmitoylphosphoglycerol (DPPG), that is known to induce amyloid aggregation.[76−79] Figure 4A shows the achiral *ssp* spectra of hIAPP at the air/water interface under the following three conditions: hIAPP solutions (1) without DPPG

Scheme 6. Interactions of Islet Amyloid Polypeptide with Lipid Molecules at the Air/Water Interface Probed by Vibrational SFG Spectroscopy. Reprinted from ref 50. Copyright 2010 American Chemical Society.

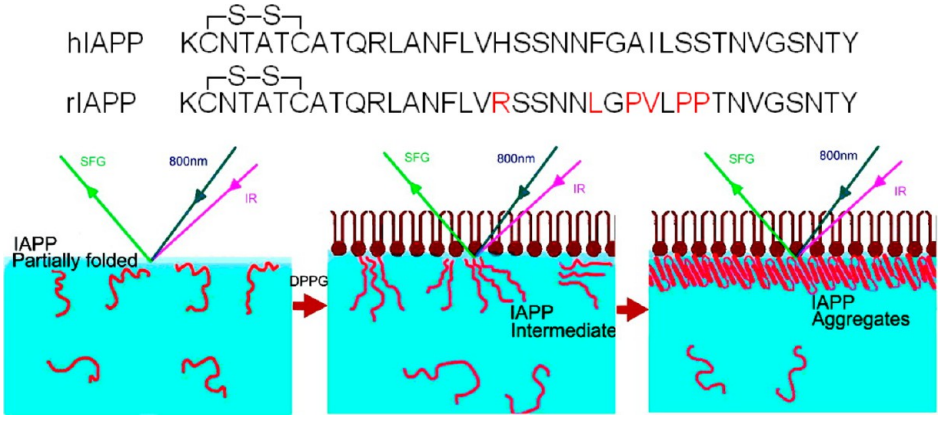

DOI: 10.1021/jp508926e
J. Phys. Chem. B 2015, 119, 2769−2785

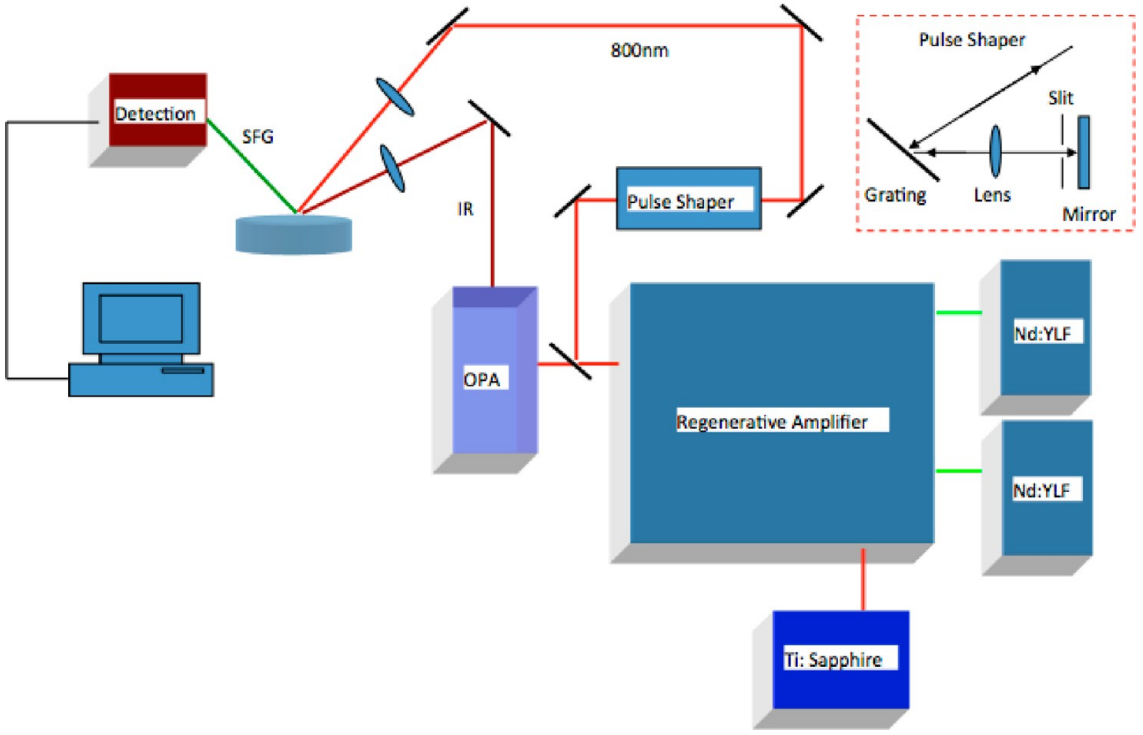

Figure 3. SFG Spectrometer. The spectrometer is seeded by a Ti:sapphire oscillator and pumped by two solid-state laser (Nd:YLF) to provide a 6 W output from a regenerative amplifier at 800 nm with a repetition rate of 5 kHz and pulse duration of 120 fs. The 6 W output is split into two beams each at 3 W. One 3 W beam is stretched to ∼2 ps by a home-built pulse shaper and used as the visible input beam for the SFG experiments. The other 3 W beam is used to pump an automated optical parametric amplifier (OPA) that generates IR pulses with broad bandwidth, 150−250 cm^{-1} in the mid-IR region. The typical power of the 800 nm and broad bandwidth IR beams are ∼135 and 10 mW, respectively, with corresponding incident angles of 56° and 69°. The SFG beam reflected from the sample surface is spectrally dispersed by a monochromator and then detected by a CCD.[63]

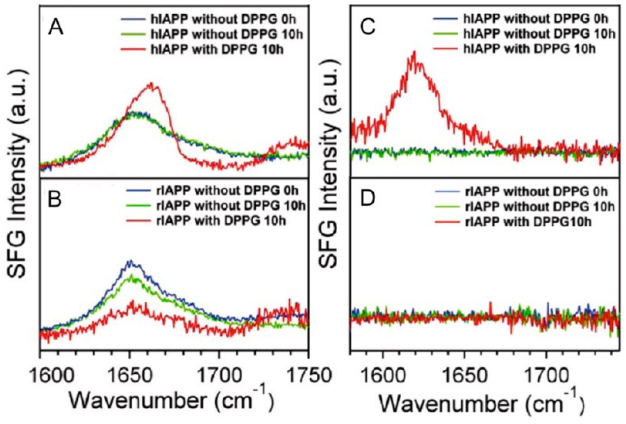

Figure 4. SFG spectra of human islet polypeptide (hIAPP) and rat islet polypeptide (rIAPP) in the amide I region at the air/water interface. Achiral *ssp* spectra of (A) hIAPP and (B) rIAPP. Chiral *psp* spectra of (C) hIAPP and (D) rIAPP. Blue: spectra taken at t = 0 h without negatively charged dipalmitoylphosphoglycerol (DPPG). Green: spectra taken at t = 10 h without DPPG. Red: spectra taken at t = 10 h after addition of DPPG. Reprinted from ref 50. Copyright 2010 American Chemical Society.

(blue), (2) incubated without DPPG for 10 h (green), and (3) incubated for 10 h with DPPG (red). In the absence of DPPG, the achiral amide I spectrum does not change regardless of incubation. However, in the presence of DPPG, the achiral spectrum shows not only an additional peak at ∼1740 cm^{-1} due to the carbonyl group in DPPG but also a shift in the amide I peak. Since the amide I frequency is sensitive to protein secondary structures (Table 1), the shift suggests that DPPG induces changes in secondary structures of hIAPP at the interface. Figure 4B shows the results of the same experiments, except that hIAPP is replaced by rIAPP that does not aggregate. Even in the presence of DPPG, the amide I peak of rIAPP does not shift, suggesting that the secondary structures of rIAPP do not change. We conclude from Figure 4 (panels A and B) that DPPG induces conformational changes in hIAPP but not in rIAPP.

We repeated the above experiments using chiral SFG. Figure 4C shows that the chiral *psp* spectra of hIAPP are silent in the absence of DPPG both before and after a 10 h incubation. However, the spectrum of hIAPP after incubation with DPPG shows an amide I peak centered at 1620 cm^{-1} and a shoulder around 1660 cm^{-1}. The fitting of these peaks is not included in Figure 4C but is presented in Figure 12C. The low (1620 cm^{-1}) and high (1660 cm^{-1}) frequency amide I bands are characteristic amide I B mode and amide I A mode of parallel β-sheets, respectively.[24,25] Hence, the results reveal lipid-induced formation of parallel β-sheets. When hIAPP is replaced with rIAPP, this lipid-induced 1620 cm^{-1} peak is absent. Hence, rIAPP does not fold into β-sheet structures upon interactions with DPPG. We conclude that DPPG induces formation of parallel β-sheet structures at the air/water interface in hIAPP but not rIAPP.

There are two exciting observations in the above experiments that reveal advantages of chiral SFG over conventional vibrational methods in probing protein structures. First, the chiral amide I peaks in chiral SFG spectrum of hIAPP (Figure 4C) is with zero background, implying that chiral SFG is background-free from water solvent. Because the bending modes

DOI: 10.1021/jp508926e
J. Phys. Chem. B 2015, 119, 2769−2785

of H_2O is in the ~1600 cm^{-1} region overlapping with the amide I vibrational frequencies, conventional vibrational studies of proteins requires the use of D_2O as a solvent. However, since water molecules are achiral, the water bending background is muted in chiral SFG spectra. Hence, H_2O can be used as a solvent, eliminating potential isotopic perturbations to the H-bonding interactions in proteins. Second, each achiral spectrum shown in Figure 4A contains the amide I bands, suggesting the presence of the proteins at the interface. However, the chiral SFG spectra are silent in all the chiral spectra except the one for hIAPP in folded β-sheet structures. These observations demonstrate that only proteins folded in chiral secondary structures are visible to chiral SFG, which further eliminate background from unfolded proteins, simplifying spectral deconvolution.

Aside from the static SFG spectra, we also obtained the time-dependent achiral (*ssp*) and chiral (*psp*) spectra of hIAPP upon interactions with DPPG at the air/water interface.[50] Figure 5A shows the amide I band in the achiral SFG spectra gradually shifts, while Figure 5B shows the intensity of the amide I band in chiral SFG spectra gradually increases. The results suggest that the aggregation process happens on the timescale of hours under our experimental conditions, demonstrating that chiral SFG can also be used to study kinetics of amyloid aggregation at interfaces in situ and in real time.

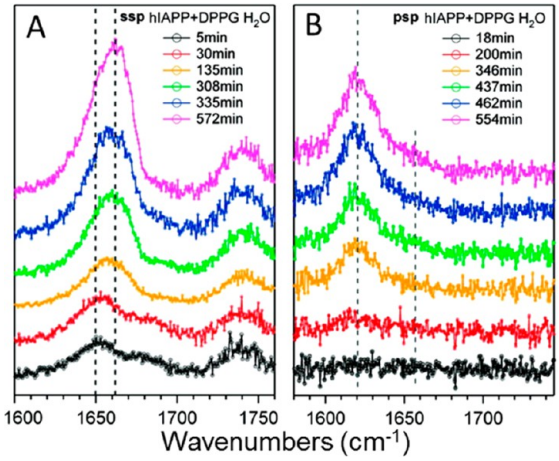

Figure 5. Time-dependent chiral and achiral SFG spectra in the amide I region of human islet polypeptide (hIAPP) at the air/water interface. (A) Achiral *ssp* spectra and (B) chiral *psp* spectra taken after addition of negatively charged dipalmitoylphosphoglycerol (DPPG) at t = 0. Reprinted from ref 50. Copyright 2010 American Chemical Society.

In our subsequent hIAPP studies, the most exciting results came from the use of the peptide N−H stretch vibrational band for probing the aggregation kinetics.[49] We performed the same experiments as described in Scheme 6 but tuned the incident IR beam to the N−H stretch vibration region at ~3200 cm^{-1}. At t = 0, we added DPPG and started monitoring the chiral SFG spectra. The N−H stretch signal gradually increases, reaches a maximum at ~3 h, and then disappears at ~10 h (Figure 6A). What is the origin of the chiral N−H stretch signal? To address this question, we first performed two control experiments, in which DPPG was not added (Figure 6B) and hIAPP was replaced with rIAPP (Figure 6C). In both experiments, the transient N−H stretch chiral signal was not observed. The results suggest that the chiral N−H stretch signal is due to an intermediate of the aggregation process.

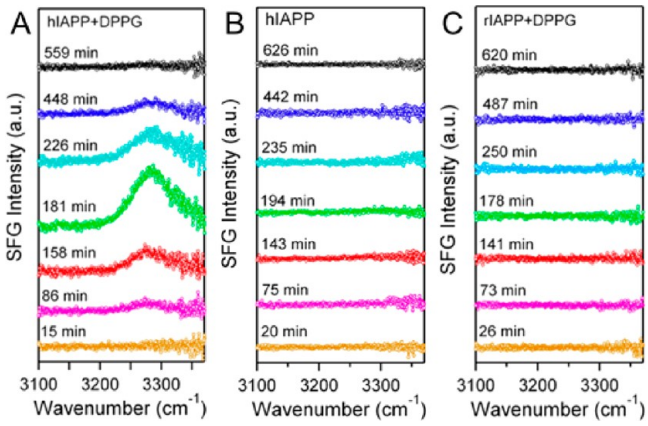

Figure 6. Time-dependent chiral SFG spectra of human islet polypeptide (hIAPP) and rat islet polypeptide (rIAPP) in the N−H stretch region at the air/water interface. (A) hIAPP with an addition of negatively charged dipalmitoylphosphoglycerol (DPPG) at t = 0. (B) hIAPP without an addition of DPPG. (C) rIAPP with an addition of DPPG at t = 0.

Then, we compared the kinetics of the N−H signals with that of the amide I signals (Figure 7).[49] We first tuned the IR beam to the N−H stretch region and monitored the N−H stretch signals. After we detected appreciable N−H stretch signal (~1−2 h), we tuned the IR frequency to the amide I region and took an amide I spectrum, which does not show any amide I signal (Figure 7). Then, we tuned the frequency back to the N−H stretch region (~4−5 h) and continued monitoring the N−H stretch signals. When the N−H stretch signal completely vanished, we tuned the IR frequency back to the amide I region (~10 h) and observed the 1620 cm^{-1} peak characteristic of parallel β-sheet structures. The results suggest that the N−H stretch signal is due to an

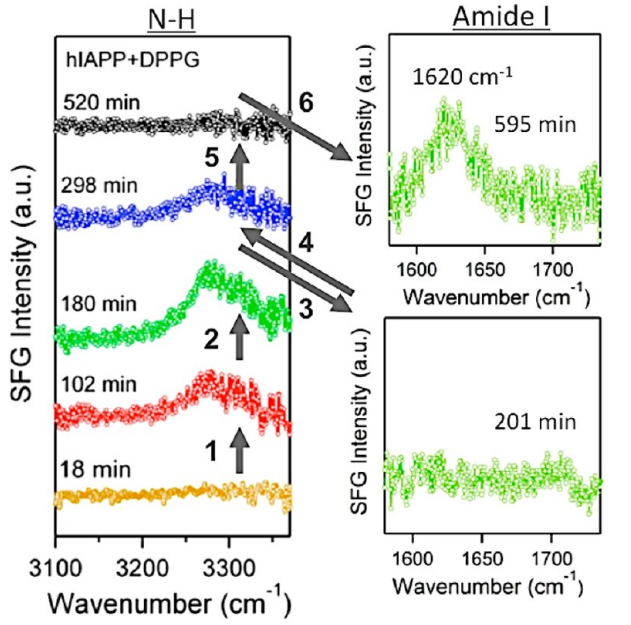

Figure 7. Chiral SFG spectra taken as a function of time in the N−H stretch and amide I regions of one sample of human islet polypeptide (hIAPP) at the air/water interface after dipalmitoylphosphoglycerol (DPPG) is added at t = 0. Sequential acquisition of spectra: N−H stretch (18, 102, and 180 min), amide I (201 min), N−H stretch (298 and 520 min), and amide I (595 min).

DOI: 10.1021/jp508926e
J. Phys. Chem. B 2015, 119, 2769−2785

intermediate that forms and then disappears before formation of the parallel β-sheets.

To further examine the origin of the chiral N−H stretch signals, we obtained additional kinetic data by monitoring the chiral SFG spectra of hIAPP in both the N−H stretch and amide I regions separately upon addition of DPPG at the air/water interface (Figure 8A).[49] We repeated the experiments for at least three times. In the first 3 h, the N−H stretch intensity starts building up, while the amide I band remains silent. At 3−4 h, the N−H stretch intensity reaches the maximum when the amide I band begins to pick up the intensity. At ∼10 h, the N−H band completely disappears and the amide I intensity reaches the maximum. Figure 8B shows the intensity of the N−H stretch and amide I bands as a function of time with three kinetic curves for the N−H stretch (red) and three for the amide I band (blue) for three sets of data. The curves clearly show that N−H stretch band increases and then disappears before the amide I band starts increasing in intensity and then reaches the maximum. While the amide I band at 1620 cm^{-1} is characteristic of parallel β-sheets, the origin of the N−H stretch band remains to be revealed. Nonetheless, previous biophysical studies revealed that hIAPP first adsorbs on lipid membrane and folds into α-helical structures before converted into β-sheet structures (Scheme 5).[22,71] Thus, it is reasonable to hypothesize that the chiral N−H stretch band comes from the α-helical intermediates.

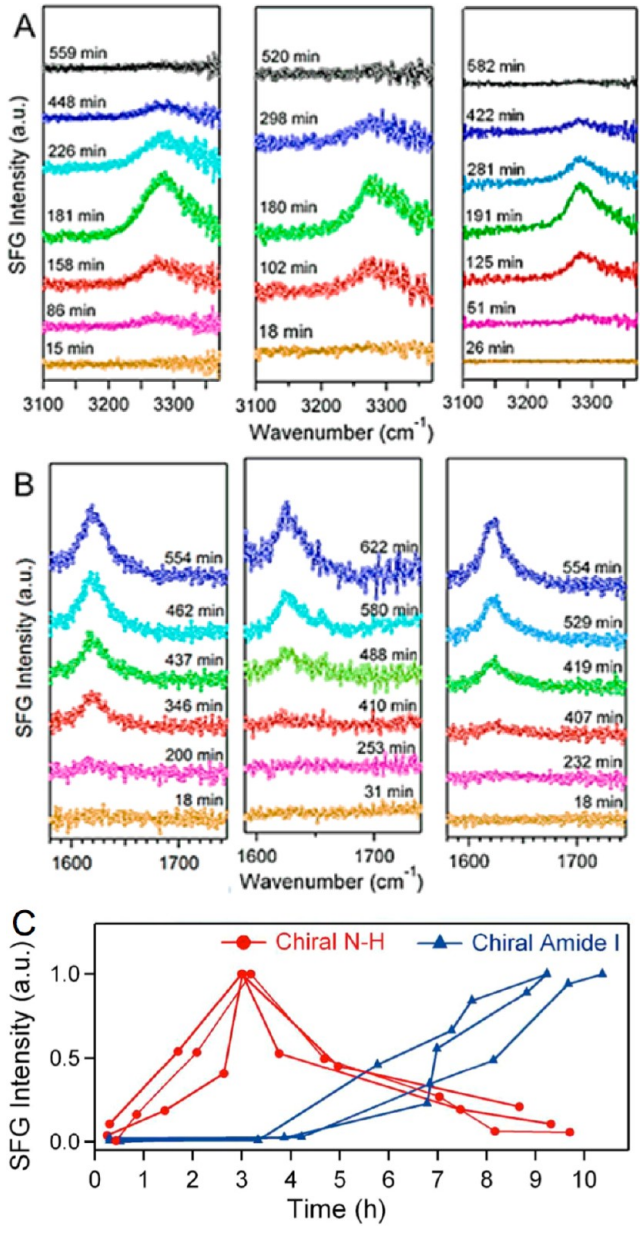

Figure 8. Time-dependent changes in chiral SFG signals in the amide I and N−H stretch vibrational regions. Time-dependent spectra in triplicate for the (A) N−H stretch and (B) amide I of human islet polypeptide (hIAPP) at the air/water interface. Dipalmitoylphosphoglycerol (DPPG) is added at t = 0. (C) Time-dependent intensity of chiral SFG signals: chiral N−H stretch (red) and chiral amide I (blue). Panel C reprinted from ref 49. Copyright 2011 American Chemical Society.

However, chiral N−H stretch spectra of proteins had not been reported prior to our studies. Hence, our attempt to validate the assignment to α-helical structures is to obtain the chiral N−H stretch spectra of model systems that are known to form α-helical structures at interfaces. We chose three model proteins (Figure 9). First, the LKα14 peptide with the sequence of $(LKKLLKL)_2$

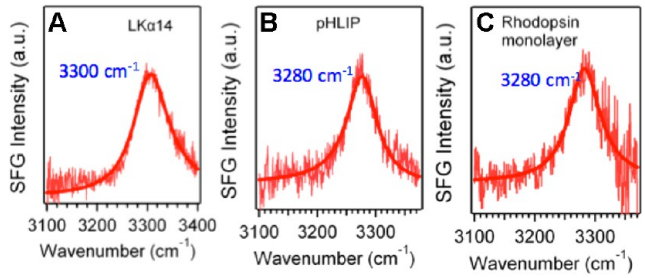

Figure 9. Chiral SFG spectra of model α-helical structures. (A) LKα14, (B) pH low insertion peptide (pHLIP), and (C) rhodopsin. Reprinted from ref 49. Copyright 2011 American Chemical Society.

was designed and shown by the DeGrado group to form α-helical structures at the air/water interface.[81] Second, the pH low insertion peptide (pHLIP) has the sequence taken from helix 3 of bacteriorhodopsin that retains an α-helical structure in an amphiphilic environment.[82,83] Finally, rhodopsin is a model system for G protein-coupled receptors with the characteristic 7-helical transmembrane structure,[7,84] which can form a stable monolayer at the air/water interface in the presence of detergent by careful control of surface pressure.[19] We obtained the chiral SFG spectra of these three model systems (Figure 9). They all show the N−H stretch vibrational band. On the basis of these results, we propose that the chiral N−H stretch is due to α-helical structure formed by hIAPP as an intermediate during the initial amyloid aggregation process on membrane surfaces. Thereby, we provide the simplest interpretation of our kinetic data (Figure 8): hIAPP first adsorbs onto the interface as disordered structure and then folds into α-helical structures before converting into β-sheet aggregates in the timescale of hours under our experimental conditions.

The above hIAPP studies have several implications in applying chiral SFG for amyloid research important in understanding a number of amyloid diseases, such as Alzheimer's and Parkinson's diseases.[67−69] First, chiral SFG can be useful for investigating the molecular mechanism of amyloid aggregation. The 1620 cm^{-1} signal detected by chiral SFG could be a unique second-order optical property of amyloid proteins without the use of spectroscopic or isotopic labels. Thus, this chiral SFG signals could be useful in detecting amyloid aggregation, especially in the

DOI: 10.1021/jp508926e
J. Phys. Chem. B 2015, 119, 2769−2785

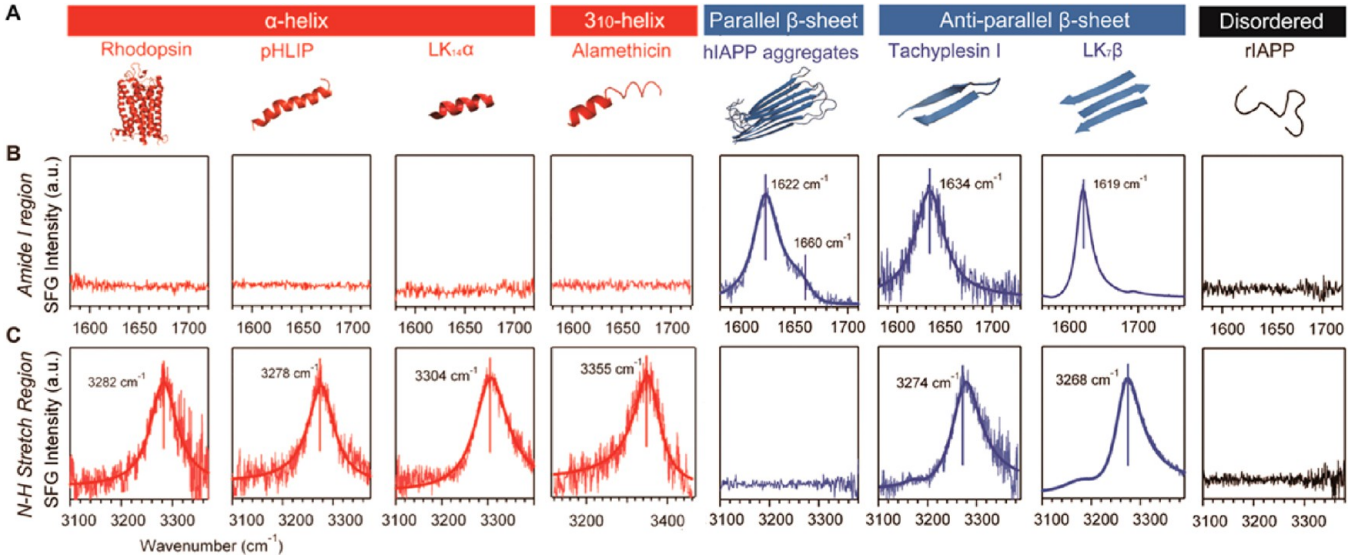

Figure 10. Chiral N−H stretch and amide I SFG spectra for a series of model proteins and peptides with schematic structures. (A) The secondary structures under study. (B) The chiral amide I SFG spectra. (C) The chiral N−H stretch spectra. Partially reprinted from ref 55. Copyright 2014 American Chemical Society.

early stages on membrane surfaces. Second, the chiral N−H stretch detected by chiral SFG is assigned to α-helical structures. For the first time, without interference from bulk contribution and the use of spectroscopic labels, the chiral SFG method allows validation of the working model, in which α-helical structures are proposed as an intermediate of the amyloid aggregation (Scheme 5). This also suggests that chiral SFG can be used to follow the kinetics of amyloid aggregation at the early stages on membrane surfaces. Thus, it can be further applied to study the molecular mechanism by exploring effects of various factors (e.g., surface charges, electrolyte concentration, and lipid head groups and carbon chains). In developing drug molecules, inhibiting a particular step in the aggregation process on membrane surfaces[85] (e.g., the conversion from α-helical structures to β-sheets), chiral SFG can provide a unique tool to evaluate the effect of drug candidates on the particular step.

In conclusion, the results of the hIAPP studies have demonstrated chiral SFG as a label-free, background-free method for studying changes in protein conformations at interfaces in situ and in real time. The success of combining chiral N−H stretch and amide I vibrational SFG signals for characterization of changes in protein secondary structures led us to ask the next question. Can chiral SFG provide optical signatures for distinguishing other protein secondary structures at interfaces?

4. CHIRAL SFG FOR CHARACTERIZATION OF PROTEIN SECONDARY STRUCTURES

To answer the above question, we obtained a series of chiral SFG spectra of model peptides and proteins in α-helix, 3_{10}-helix, antiparallel β-sheet, parallel β-sheet, and disordered structures.[49,51−53,55] We took the N−H stretch and amide I spectra using chiral SFG at the air/water interface either in the presence or absence of lipid or detergent in the N−H stretch and amide I regions (Figure 10).

We first compare the spectra of α- and 3_{10}-helices (Figure 10). We used rhodopsin,[84,86] pHLIP,[82,83] and LKα14[31,38,81] as model systems for α-helices and alamethicin for 3_{10}-helix.[8,87,88] All chiral SFG spectra show prominent N−H stretch bands but no amide I band. The N−H stretch frequencies for α-helical and 3_{10}-helical structures are different by more than 50 cm^{-1}. This large shift may not be surprising because protein secondary structures are stabilized by H bonds formed between the peptide N−H and C═O groups. Since 3_{10}-helices have three amino acids in one helical turn instead of 3.6 amino acids in α-helices, the H-bonding environments at the peptide N−H groups are expected to be different, which in turn can modulate and shift the N−H stretch frequency.

We then compare the chiral SFG spectra of antiparallel and parallel β-sheets (Figure 10). For antiparallel β-sheets, we used tachyplicin I[89−91] and LK$_7\beta$[81] as model systems, of which chiral SFG spectra show both N−H stretch and amide I signals with the N−H stretch peak centered at 3270 cm^{-1} and the amide I peak centered at 1620−1630 cm^{-1}. For parallel β-sheets, the spectra of hIAPP aggregates show only the amide I band but not the N−H band. At first glance, this result suggests that chiral SFG could be easily used to distinguish parallel β-sheet from antiparallel β-sheet. However, we later found that the orientation angle of the β-strand in hIAPP at the air/water interface is at ∼45° from the surface (see next section).[54] In an ongoing study, we have derived from the SFG theory that the 45° orientation should mute the N−H stretch signal and indeed observed the N−H stretch signals in the chiral SFG spectrum of hIAPP aggregates on the glass slide, where the β-strands are expected to be parallel to the surface due to amphiphilic interactions. Moreover, there is a shoulder peak at ∼3180 cm^{-1} in the spectra of antiparallel β-sheets. This N−H stretch peak had not been reported prior to our studies.[53] We further obtained the amide I and amide II chiral SFG spectra and showed that this peak is the combination band of the amide I and amide II bands, which was also supported by vibrational analysis using quantum chemistry calculations, as discussed in Fu et al.[53]

Finally, we show that disordered structures do not give any chiral SFG signal in either the N−H stretch region or the amide I region (Figure 10). We used rIAPP as a model system. The spectra are silent in both the N−H stretch and amide I regions. One may argue that the peptide is not present at the interface. However, the achiral amide I and N−H stretch spectra of rIAPP (Figure 11) show the amide I spectrum peak at 1655 cm^{-1},

DOI: 10.1021/jp508926e
J. Phys. Chem. B 2015, 119, 2769−2785

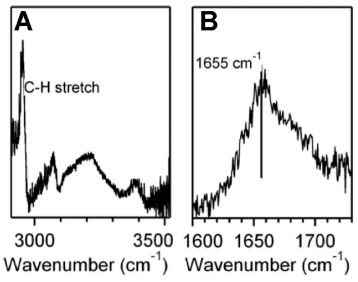

Figure 11. Achiral SFG spectra of rat islet amyloid polypeptide (rIAPP) taken using *ssp* polarization. (A) N−H stretch region. (B) Amide I region. Reprinted from ref 49. Copyright 2011 American Chemical Society.

suggesting that rIAPP is at the interfaces. Hence, disordered structures do not give a detectable chiral SFG signal under our experimental conditions.

The results presented in Figure 10 show the unique selectivity of chiral SFG signals to the N−H stretch and amide I modes in various secondary structures. A theoretical description about this selectivity has been explored by Simpson and co-workers,[43,44] Wang and co-workers,[45] and our group recently.[55] However, a comprehensive and quantitative theory is to be developed to fully incorporate three important factors that determine the chiral SFG response of amide groups of protein secondary structures: orientation, molecular symmetry, and vibrational coupling. We are in the process of developing such theoretical descriptions for quantitative interpretation of the chiral SFG spectra (Figure 10).

Figure 10 presents the series of chiral SFG spectra of model peptides and proteins in various secondary structures. These spectra show the vibrational signatures that are characteristic of the secondary structures. The achiral spectra of some of the model systems have also been examined, as reported in Fu et al.[49] The achiral spectra show the generally broad amide I bands at the interface regardless of their secondary structures and the O−H stretch background from water solvent in the N−H stretch region. Taken together, the results demonstrate the potential of using chiral SFG as a label-free vibrational method for characterizing protein structures in situ and in real time at interfaces. The applications of these vibrational signatures could be similar to those of circular dichroism signatures for distinguishing protein secondary structures in aqueous solution but with surface selectivity.

Our results show a few advantages that can make the chiral SFG method complementary to conventional techniques in characterization of protein secondary structures. Chiral SFG is free of water background, and thus H_2O can be used as the solvent instead of D_2O. Moreover, chiral SFG can be used to probe not only amide I bands but also the N−H stretch vibrational bands, providing more information about vibrational structures to reveal protein secondary structures. In addition, the chiral SFG spectra of helical structures is silent in the amide I region, making the deconvolution of amide I spectra relatively simple. This could be particularly useful in resolving secondary structures in complex protein systems.

Moreover, chiral SFG can be used to report the peptide N−H stretch frequency. As discussed earlier, the N−H stretch frequency can reveal H-bonding environments of the N−H groups in peptides and, thereby, provide information about protein secondary structures. However, the peptide N−H stretch had rarely been used for protein characterizations. The reason is that the N−H stretch overlaps with the water O−H stretch, which can overwhelm the N−H stretch signals. The use of D_2O cannot solve the problem because protons in the backbone N−H can be exchanged with deuterium. In this case, the N−D stretch signal is detected over the water O−D stretch background. Chiral SFG can uniquely overcome this problem because achiral water molecules do not contribute to the background. Hence, the peptide N−H stretch frequency can be measured accurately, providing an additional tool for probing protein secondary structures.

Aside from selectivity to secondary structures, chiral SFG also has the sensitivity to interfaces under the conditions where electronic resonance is absent and the anisotropic chiral interface is in contact with isotropic bulk media.[55] This condition is satisfied in a number of important systems, such as proteins in aqueous solution interacting with lipid membrane, biomarkers in liquid media being detected by biosensors, and protein self-assembly from aqueous solution onto inorganic solid substrates (Figure 1). Therefore, chiral SFG can be used to attack a wide range of fundamental and engineering problems. In the next section, we will summarize our recent applications and method developments of chiral SFG for studying proteins at interfaces.

5. APPLICATIONS OF CHIRAL SFG FOR PROBING PROTEINS AT INTERFACES

We have recently performed three chiral SFG studies, as described below, to develop new tools for probing orientation, proton exchange and folding kinetics of proteins at interfaces.

First, we measured the orientation of hIAPP aggregates at the lipid/water interface.[54] Knowledge about amyloid orientation on membrane surfaces is crucial for understanding the pathogenic mechanism of amyloid diseases because amyloid aggregation at the early stages has been proposed to disrupt membrane integrity, leading to cytotoxicity.[70,72,73,75,92,93] We analyzed the amide I chiral and achiral spectra of the hIAPP aggregates at the lipid/water interface (Figure 4, panels C and D).[54] The achiral SFG spectrum does not show an amide I B band at 1620 cm^{-1} in Figure 4D, indicating that the dipole for the amide I B mode lies flat on the surface (Figure 12A), implying that the long axis of the β-sheet is parallel to the surface (i.e., $\theta = 90°$) (Figure 12B). The chiral SFG spectrum with high signal-to-noise level is shown in Figure 12C, from which the ratio of intensity of amide I B mode ($I_{SFG,B}$) at ~1620 cm^{-1} to that of amide I A mode ($I_{SFG,A}$) at ~1660 cm^{-1} can be measured. This ratio can be expressed as a function of hyperpolarizability (β) tensor elements and orientation angle (ψ) defined by the laboratory coordinates (x, y, z) and molecular coordinates (a, b, c) shown in Figure 12B:

$$\frac{I_{SFG,B}}{I_{SFG,A}} = \left|\frac{\chi^{(2)}_{psp,B}}{\chi^{(2)}_{psp,A}}\right|^2 = \left|\langle\tan^2\psi\rangle\frac{\beta_{bca,B}}{\beta_{acb,A}} + (1 - \langle\tan^2\psi\rangle)\frac{\beta_{bca,B}}{\beta_{acb,A}}\right|^2 \quad (6)$$

where $\chi^{(2)}_{psp,R}$ and $\chi^{(2)}_{psp,B}$ are the second-order susceptibility of A and B modes, respectively, and $\beta_{ijk,A}$ and $\beta_{ijk,B}$ (i, j, k = a, b, c) are the tensor elements of hyperpolarizability of the β-sheet IAPP aggregates for the amide I A and B modes, respectively. Since the intensity ratio can be measured (Figure 12C), if the hyperpolarizability tensor elements are known, the orientation of the β-sheet aggregates can be obtained using eq 4. We collaborated with Batista and Xiao, who built a molecular model for the hIAPP

DOI: 10.1021/jp508926e
J. Phys. Chem. B 2015, 119, 2769−2785

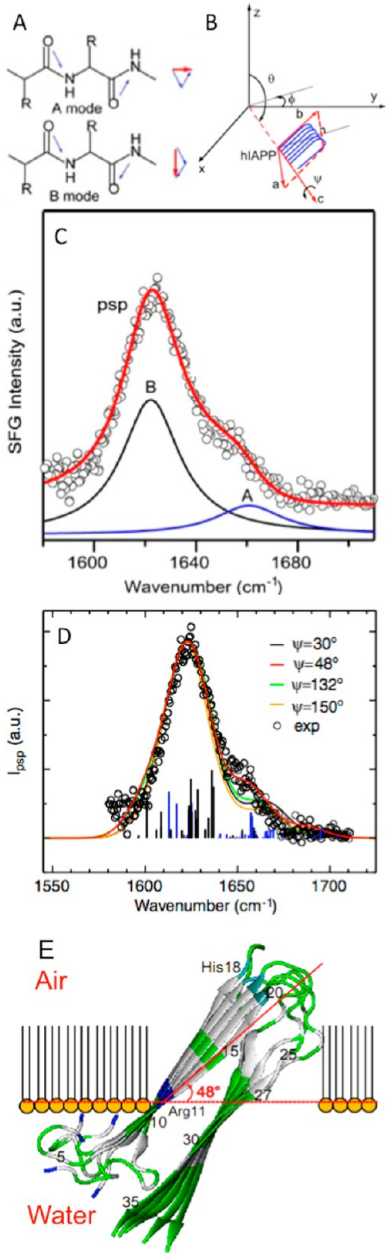

Figure 12. Comparisons of experimental and in situ simulated chiral amide I spectra of hIAPP aggregates at the air/water interface with DPPG lipid. (A) Net transition dipole of amide I A and B modes. (B) Molecular coordinates (a, b, c) and laboratory coordinates (x, y, z). (C) The experimental spectrum fitted into A mode (~1660 cm^{-1}) and B mode (~1620 cm^{-1}). (D) Comparison of experimental (circle) and simulated spectra at various twist angles (ψ). (E) A model of hIAPP at the air/water interface with DPPG. Color code for amino acids: gray (hydrophobic) and green (hydrophilic). Reprinted with permission from ref 54. Copyright 2012 Elsevier.

aggregates and implemented the divide-and-conquer method to perform in situ calculation to obtain the hyperpolarizability. They further simulated the chiral SFG amide I spectrum for a comparison with the experimental results (Figure 12D). The comparison led to a conclusion that the β-strand of the hIAPP aggregate orients at ~45° from the surface (Figure 12E), which agrees with a number of biochemical and biophysical studies of hIAPP interacting with biomembrane.[10,70,92,94−96]

Our second study involves using the chiral N−H stretch of protein backbone for monitoring proton exchange in proteins at interfaces.[51] Kinetics of proton exchange in proteins in bulk solutions has been studied using solution NMR and mass spectrometry.[97−100] The kinetics can reveal solvent exposure of proteins,[101] dynamics of interactions between water and proteins,[102] and H-bonding interactions in proteins.[103] Since the N−H (or N−D) stretch of peptide backbones detected by chiral SFG is free of water O−H (or O−D) background, monitoring the changes in the intensity of N−H or N−D stretch using chiral SFG upon H_2O/D_2O solvent exchange can reveal the kinetics of proton exchange. We used $LK_7\beta$ as a model system that forms parallel β-sheets at the air/water interface.[22,50,70,104] We monitored the intensity of $LK_7\beta$'s N−D stretch at the air/water interface upon addition of D_2O to H_2O solution. We found that the chiral N−D signals gradually increase (Figure 13A).

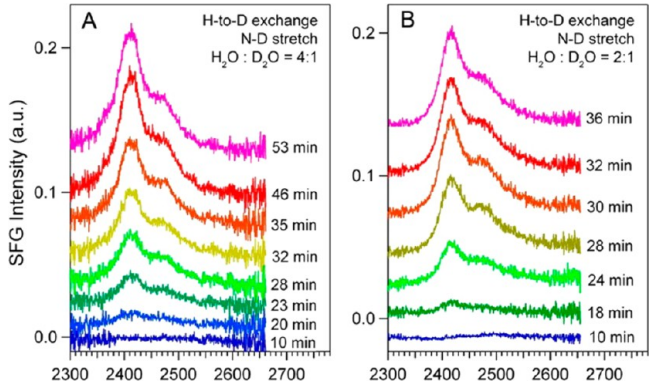

Figure 13. Time-dependence of chiral SFG signals in the N−H and N−D stretch regions after H_2O/D_2O solvent exchange at $t = 0$. (A) The H-to-D and (B) D-to-H exchange in $LK_7\beta$ at the air/water interface. Reprinted from ref 53. Copyright 2013 American Chemical Society.

Similarly, addition of H_2O to D_2O solution of $LK_7\beta$ leads to an increase in the N−H intensity (Figure 13B). Figure 13 shows that the rate of D-to-H exchange is higher than that of H-to-D exchange, implying that breaking the O−H (or O−D) bonds in water rather breaking the N−H (or N−D) bonds in $LK_7\beta$ is the rate-determining step of the proton-exchange process, as discussed in Fu et al.[53] These studies demonstrate a new application of chiral SFG, probing proton exchange in protein backbones in situ and in real time at interfaces, which could be particularly useful in studying membrane proteins, such as solvent exposure and H-bonding interactions in lipid membrane environments.

Finally, we extended our chiral vibrational studies of proteins from the amide I and N−H stretch to the C−H stretch vibrational mode.[56] We probed the self-assembly process of $LK_7\beta$ into antiparallel β-sheet structures at the air/water interfaces. We first observed chiral C−H stretch signals from $LK_7\beta$ (phosphate 10 mM, pH 7.4), as shown in Figure 14, indicating the formation of macroscopic chiral secondary structures at the interface. We fitted the C−H stretch spectrum and assigned the peaks to the methyl and methylene stretches (Figure 14), as reported in Wang et al.[56] The methyl stretches originate from the methyl groups in the leucine residues, while the methylene stretches can originate from both the lysine and leucine residues, with possible larger contributions from the β-carbon due to its proximity to the peptide backbones in macroscopic chiral arrangements. Then, we denatured the proteins by lowering the pH to 1.2 and

DOI: 10.1021/jp508926e
J. Phys. Chem. B 2015, 119, 2769−2785

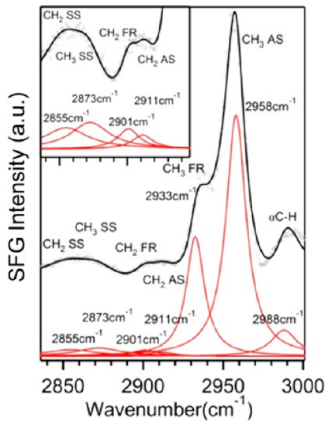

Figure 14. Chiral SFG spectrum of LK$_7\beta$ and spectral fitting in the C−H stretch region: symmetric stretch (SS) of CH_2 (2855−2859 cm^{-1}), SS of CH_3 (2873−2875 cm^{-1}), Fermi resonance (FR) of CH_2 (2891−2901 cm^{-1}), antisymmetric (AS) stretch of CH_2 (2909−2911 cm^{-1}), FR of CH_3 (2933−2936 cm^{-1}), AS of CH_3 (2958−2959 cm^{-1}), and C_α−H stretch of the peptide (2984−2988 cm^{-1}).[105−107] Reprinted from ref 56. Copyright 2013 American Chemical Society.

observed that the chiral C−H stretch SFG signal disappears. Subsequently, we triggered the self-assembly process by neutralizing the pH and monitored the chiral C−H stretch signals. The chiral C−H stretch signals gradually increase (Figure 15A), but the achiral C−H stretch signal fluctuates instead (Figure 15B). Since the achiral SFG spectrum includes contributions of signals from all protein molecules in folded and unfolded structures in various orientations, we propose that some of these structures and/or orientations in the inhomogeneous population could instantaneously dominate the signal

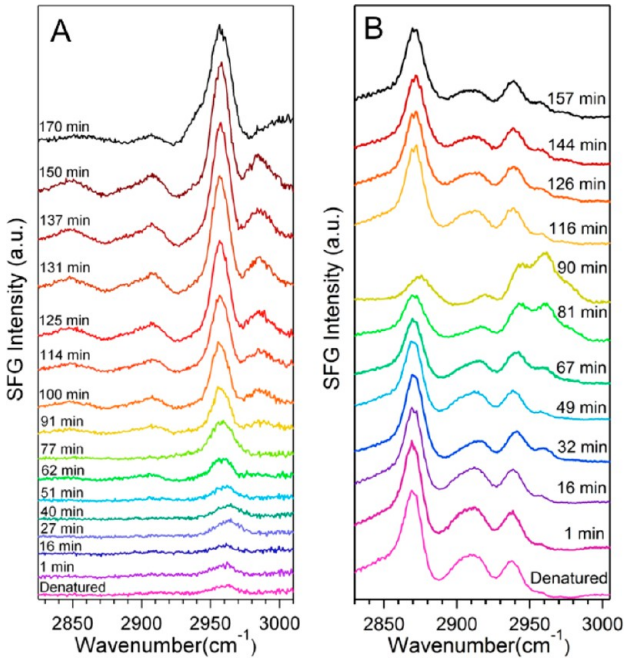

Figure 15. Time-dependent (A) chiral (*psp*) and (B) achiral (*ssp*) SFG spectra in the C−H stretch region during the self-assembling process of LK$_7\beta$ at the air/water interface. The antiparallel β-sheet LK$_7\beta$ at the interface was first denatured at pH 2. Then, NaOH was added to neutralize the pH to trigger the self-assembly process at $t = 0$. Reprinted from ref 56. Copyright 2013 American Chemical Society.

contribution, leading to the fluctuation. In contrast, chiral SFG is only sensitive to the folded chiral LK$_7\beta$ in antiparallel β-sheet structures. Because of LK$_7\beta$'s amphiphilic property, the hydrophobic leucine residues point to the air phase and the hydrophilic lysine residues point to the water phase. Thus, the folded structures are expected to be more homogeneous in orientation and more ordered. Hence, the intensity of chiral SFG signals depends mostly on the population of folded LK$_7\beta$. Thus, as ordered antiparallel β-sheets assemble at the interface, the chiral SFG signals increase gradually. These results reveal that chiral SFG could be more reliable than achiral (conventional) SFG for monitoring formation of chiral structures at interfaces. Moreover, the use of C−H stretch for probing kinetic process is simpler than the use of amide I and N−H stretch in SFG experiments because the energy in the C−H region is generally higher. Also, atmospheric H_2O and CO_2 will not attenuate the IR beam in the C−H stretch frequency; thus, it is not necessary to purge the IR optical path with dry nitrogen. Since C−H stretches are ubiquitous in organic compounds, our studies imply applications of chiral SFG to study interfacial structures of a wide range of native and synthetic biopolymers and supramolecular structures.

6. SUMMARY AND OUTLOOK

In summary, we have presented our recent experimental work on developing chiral SFG vibrational spectroscopy for studying proteins at interfaces. Our applications of chiral SFG to the aggregation process of hIAPP at the lipid/water interfaces demonstrate the ability of chiral SFG to monitor kinetics of protein conformational changes at interfaces without the use of spectroscopic or isotopic labels. The chiral SFG method provides a set of background-free optical vibrational signatures for in situ and real-time characterization of protein secondary structures at interfaces. These chiral SFG vibrational signatures can be used to probe orientation and proton exchange of proteins at interfaces. The extension of the method from N−H stretch and amide I vibrational modes to the C−H stretching mode illustrates the potential of the method in probing not only proteins but also other native biopolymers, such as polysaccharides, DNA, and RNA, as well as synthetic chiral polymers and supramolecular structures.

Our work has revealed the potential of chiral SFG in addressing a variety of important fundamental and engineering questions. For example, it can be used to observe protein folding at interfaces in situ and in real time. While protein folding in aqueous solution has long been a subject of interest, relatively few experimental data are available for interfaces. Hence, chiral SFG is expected to have an impact on developing and testing hypotheses for describing protein folding at 2D surfaces. Second, as chiral SFG can be used to measure orientation of protein secondary structures at interfaces, it can be used to study protein functions at interfaces that involve changes in secondary structures and orientation. This could be useful in probing transmembrane proteins and peripheral membrane proteins in addressing a number of biological processes (Figure 1), such as signal transduction, molecular transport, and cell adhesion. The characterizations of protein secondary structures and orientation can also aid molecular design of biomaterials, drug delivery systems, biosensors, and organic/inorganic hybrid interface (Figure 1). Moreover, protein imaging in cellular environments without the use of spectroscopic probes remains challenging because label-free vibrational signals of proteins are often overwhelmed by the vibrational backgrounds of water and

DOI: 10.1021/jp508926e
J. Phys. Chem. B 2015, 119, 2769−2785

other biomolecules. Since chiral SFG is free of water background and highly selective to protein secondary structures, the potential applications of chiral SFG for protein imaging should be recognized. In fact, a similar chiral SHG method has been successfully implemented for imaging protein crystals and other bioactive molecules, demonstrating important applications in pharmaceutical industry.[108] Hence, chiral vibrational SFG microscopy, if made possible, would provide more molecular and structural information and is expected to solve a wider range of problems.

Continuous development of chiral SFG for characterizing chiral structures at interfaces require both experimental and theoretical efforts. Here, we discuss three important aspects, where physical chemists may contribute. First, the chiral SFG measurements involve picosecond and femtosecond pulsed laser, providing the time resolution for ultrafast dynamics studies. These studies introduce exciting opportunities in photochemistry and photobiology. For example, dim-light photoreceptor rhodopsin has been extensively studied by many advanced laser spectroscopic methods.[19,109−115] Nonetheless, little is known about the vibrational energy propagation process from the photoexcited retinal chromophore to the active-site protein, which consists of both α-helical and β-sheet structures.[84] What are the differences in the timescale and efficiency of vibrational energy propagating from the photoexcited chromophore to the α-helices versus to the β-sheets? Without optical vibrational signatures that can distinguish α-helices and β-sheets, this question is impossible to address. Nonetheless, the chiral vibrational signatures for protein secondary structures provided by chiral SFG (Figure 10) can potentially solve the problem.

Second, combined experimental and theoretical efforts are crucial for further developing chiral SFG into a quantitative tool. Since chiral SFG has a selection rule that is different from conventional vibrational methods and the chiral SFG signals are free of water background, it can potentially reveal detailed vibrational structures that cannot be observed using conventional vibrational methods. As an example, we observed a subtle shoulder peak in the chiral N−H spectrum of LK$_7\beta$ at the air/H_2O interface at 3178 cm^{-1} (Figure 10C),[53] which was not reported previously. Aided by in situ calculation, we assigned this shoulder peak to the combination band of amide I and amide II that we also observed using chiral SFG at 1619 and 1563 cm^{-1}, respectively.[53] This combination band could potentially be used to probe interactions between proteins and water solvent. Thus, careful characterizations of chiral SFG vibrational spectra in conjunction with theoretical calculations can potentially identify new vibrational probes for addressing fundamental problems.

Finally, quantitative analyses of chiral SFG spectra require knowledge of molecular hyperpolarizability that describes microscopic SFG responses of molecules. As shown in the studies of orientation of hIAPP aggregates at interfaces, it is pertinent to know the hyperpolarizability in order to quantitatively interpret spectra and extract orientation information. Since chiral macromolecular structures (e.g., proteins and DNA) are large molecules, vibrational analyses using in situ quantum chemistry approaches to perform calculation for the entire molecules are often impossible. Thus, approximation methods are needed, such as summation of contributions of hyperpolarizability from monomeric units in biopolymers[116−118] as well as divide-and-conquer approaches.[54] Continuous innovations in theoretical methods to improve the accuracy and reduce the cost of calculations are essential. Only when hyperpolarizability can be accurately determined can we fully explore how three important factors quantitatively determine the chiral SFG response from the chiral macromolecular structures: orientation, symmetry, and vibrational coupling. The experimental results presented here (e.g., Figure 10) will, therefore, serve as a basis for validation in continuous development of a chiral SFG theory and methods for calculating hyperpolarizability.

In conclusion, recent experimental results have demonstrated the power of chiral SFG for in situ and real-time characterizations of protein structures and potentially other chiral polymers at interfaces. Further method development requires research efforts from both experimentalists and theoreticians in physical chemistry, while further implementation of the method in addressing fundamental and engineering questions requires cross-disciplinary collaboration, where meaningful samples can be prepared and important problems can be identified. This progress is crucial in advancing chiral SFG for solving problems related to proteins and other chiral biopolymers at interfaces in biomedical research, material science, energy research, and beyond.

AUTHOR INFORMATION

Corresponding Author

*E-mail: elsa.yan@yale.edu.

Present Address

[†](L.F.) Pacific Northwest National Laboratory, 902 Battelle Boulevard, Richland, WA 99352.

Notes

The authors declare no competing financial interest.

Biographies

Elsa Yan received her BSc from the Chinese University of Hong Kong. She then obtained her Ph.D. at Columbia University, carrying out her thesis research on applications of nonlinear optics in surface chemistry in Eisenthal's Lab. Then, she was a joint postdoctoral fellow with Richard Mathies at UC Berkeley and Thomas Sakmar at Rockefeller University, where she combined Raman spectroscopy with methods in molecular biology to study the G-protein coupled receptor rhodopsin. After being a Research Assistant Professor at Rockefeller University, she joined Yale as an Assistant Professor of Chemistry in 2007 and was promoted to Full Professor in 2014. Her research is built on the foundation of using physical chemistry methods to address biological questions related to biomembrane and membrane proteins at the fundamental level.

DOI: 10.1021/jp508926e
J. Phys. Chem. B 2015, 119, 2769−2785

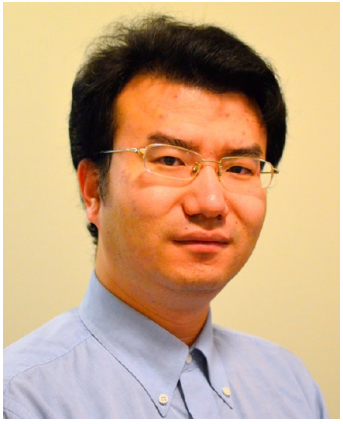

Li Fu graduated from University of Science and Technology of China (USTC) with a bachelor's degree in chemical physics in 2008. He then became a graduate student under the supervision of Elsa Yan at Yale University, developing chiral vibrational sum frequency generation spectroscopy to characterize biomolecules at interfaces. Li received his Ph.D. in 2013. He is currently a William Wiley Postdoctoral researcher at the Environmental Molecular Sciences Laboratory (EMSL) at the Pacific Northwest National Laboratory (PNNL).

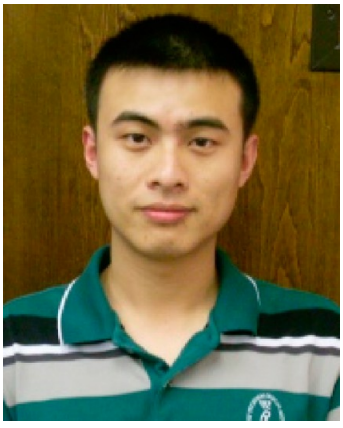

Zhuguang Wang received his B.S. in Chemical Physics from the University of Science and Technology, China, in 2010. He then joined Elsa Yan's group at Yale University to pursue his Ph.D. in chemistry. He is currently working on his thesis research in developing experimental and theoretical tools in chiral vibrational sum frequency generation spectroscopy for characterizing structures, dynamics, and orientation of biomacromolecules at interfaces, aiming to reveal molecular mechanisms of the biological processes on membrane surfaces.

■ ACKNOWLEDGMENTS

E.Y. is the recipient of the Starter Grant Award, Spectroscopy Society of Pittsburgh. This work was supported by the Yale Start-up fund and the National Science Foundation (NSF) Grant CHE 1213362. The authors thank Yuting Liu and Wei Liu (Yale University) for technical assistance.

■ REFERENCES

(1) Merianos, H. J.; Cadieux, N.; Lin, C. H.; Kadner, R. J.; Cafiso, D. S. Substrate-Induced Exposure of an Energy-Coupling Motif of a Membrane Transporter. *Nat. Struct. Biol.* **2000**, *7*, 205−209.
(2) Borst, P.; Elferink, R. O. Mammalian ABC Transporters in Health and Disease. *Annu. Rev. Biochem.* **2002**, *71*, 537−592.
(3) Keselowsky, B. G.; Collard, D. M.; García, A. J. Surface Chemistry Modulates Fibronectin Conformation and Directs Integrin Binding and Specificity to Control Cell Adhesion. *J. Biomed. Mater. Res., Part A* **2003**, *66A*, 247−259.
(4) Rosenbaum, D. M.; Rasmussen, S. G. F.; Kobilka, B. K. The Structure and Function of G-Protein-Coupled Receptors. *Nature* **2009**, *459*, 356−363.
(5) Zhang, S. G. Fabrication of Novel Biomaterials through Molecular Self-Assembly. *Nat. Biotechnol.* **2003**, *21*, 1171−1178.
(6) Castner, D. G.; Ratner, B. D. Biomedical Surface Science: Foundations to Frontiers. *Surf. Sci.* **2002**, *500*, 28−60.
(7) Li, J.; Edwards, P. C.; Burghammer, M.; Villa, C.; Schertler, G. F. X. Structure of Bovine Rhodopsin in a Trigonal Crystal Form. *J. Mol. Biol.* **2004**, *343*, 1409−1438.
(8) Bechinger, B. The Structure, Dynamics and Orientation of Antimicrobial Peptides in Membranes by Multidimensional Solid-State NMR Spectroscopy. *Biochim. Biophys. Acta, Biomembr.* **1999**, *1462*, 157−183.
(9) Luca, S.; Yau, W. M.; Leapman, R.; Tycko, R. Peptide Conformation and Supramolecular Organization in Amylin Fibrils: Constraints from Solid-State NMR. *Biochemistry* **2007**, *46*, 13505−13522.
(10) Madine, J.; Jack, E.; Stockley, P. G.; Radford, S. E.; Serpell, L. C.; Middleton, D. A. Structural Insights into the Polymorphism of Amyloid-Like Fibrils Formed by Region 20−29 of Amylin Revealed by Solid-State NMR and X-Ray Fiber Diffraction. *J. Am. Chem. Soc.* **2008**, *130*, 14990−15001.
(11) Paterson, Y.; Englander, S. W.; Roder, H. An Antibody Binding Site on Cytochrome C Defined by Hydrogen Exchange and Two-Dimensional NMR. *Science* **1990**, *249*, 755−759.
(12) Ganim, Z.; Chung, H. S.; Smith, A. W.; Deflores, L. P.; Jones, K. C.; Tokmakoff, A. Amide I Two-Dimensional Infrared Spectroscopy of Proteins. *Acc. Chem. Res.* **2008**, *41*, 432−441.
(13) Hamm, P.; Lim, M.; DeGrado, W. F.; Hochstrasser, R. M. The Two-Dimensional IR Nonlinear Spectroscopy of a Cyclic Penta-Peptide in Relation to Its Three-Dimensional Structure. *Proc. Natl. Acad. Sci. U.S.A.* **1999**, *96*, 2036−2041.
(14) Shim, S. H.; Strasfeld, D. B.; Ling, Y. L.; Zanni, M. T. Automated 2D IR Spectroscopy Using a Mid-IR Pulse Shaper and Application of This Technology to the Human Islet Amyloid Polypeptide. *Proc. Natl. Acad. Sci. U.S.A.* **2007**, *104*, 14197−14202.
(15) Strasfeld, D. B.; Ling, Y. L.; Gupta, R.; Raleigh, D. P.; Zanni, M. T. Strategies for Extracting Structural Information from 2D IR Spectroscopy of Amyloid: Application to Islet Amyloid Polypeptide. *J. Phys. Chem. B* **2009**, *113*, 15679−15691.
(16) Zanni, M. T.; Ge, N. H.; Kim, Y. S.; Hochstrasser, R. M. Two-Dimensional IR Spectroscopy Can be Designed to Eliminate the Diagonal Peaks and Expose Only the Crosspeaks Needed for Structure Determination. *Proc. Natl. Acad. Sci. U.S.A.* **2001**, *98*, 11265−11270.
(17) Maekawa, H.; Toniolo, C.; Moretto, A.; Broxterman, Q. B.; Ge, N. H. Different Spectral Sigatures of Octapeptide 3_{10} and α-Helices Revealed by Two-Dimensional Infrared Spectroscopy. *J. Phys. Chem. B* **2006**, *110*, 5834−5837.
(18) Mukherjee, P.; Kass, I.; Arkin, I.; Zanni, M. T. Picosecond Dynamics of a Membrane Protein Revealed by 2D IR. *Proc. Natl. Acad. Sci. U.S.A.* **2006**, *103*, 3528−3533.
(19) Lavoie, H.; Desbat, B.; Vaknin, D.; Salesse, C. Structure of Rhodopsin in Monolayers at the Air-Water Interface: A PM-IRRAS and X-Ray Reflectivity Study. *Biochemistry* **2002**, *41*, 13424−13434.
(20) Mendelsohn, R.; Brauner, J. W.; Gericke, A. External Infrared Reflection Absorption Spectrometry of Monolayer Films at the Air-Water Interface. *Annu. Rev. Phys. Chem.* **1995**, *46*, 305−334.
(21) Meister, A.; Nicolini, C.; Waldmann, H.; Kuhlmann, J.; Kerth, A.; Winter, R.; Blume, A. Insertion of Lipidated Ras Proteins into Lipid Monolayers Studied by Infrared Reflection Absorption Spectroscopy (IRRAS). *Biophys. J.* **2006**, *91*, 1388−1401.
(22) Lopes, D. H. J.; Meister, A.; Gohlke, A.; Hauser, A.; Blume, A.; Winter, R. Mechanism of Islet Amyloid Polypeptide Fibrillation at Lipid Interfaces Studied by Infrared Reflection Absorption Spectroscopy. *Biophys. J.* **2007**, *93*, 3132−3141.
(23) Barackov, I.; Mause, A.; Kapoor, S.; Winter, R.; Schembecker, G.; Burghoff, B. Investigation of Structural Changes of Beta-Casein and

DOI: 10.1021/jp508926e
J. Phys. Chem. B 2015, 119, 2769−2785

Lysozyme at the Gas-Liquid Interface during Foam Fractionation. *J. Biotechnol.* **2012**, *161*, 138−146.
(24) Tamm, L. K.; Tatulian, S. A. Infrared Spectroscopy of Proteins and Peptides in Lipid Bilayers. *Q. Rev. Biophys.* **1997**, *30*, 365−429.
(25) Barth, A.; Zscherp, C. What Vibrations Tell Us about Proteins. *Q. Rev. Biophys.* **2002**, *35*, 369−430.
(26) Jackson, M.; Mantsch, H. H. The Use and Misuse of FTIR Spectroscopy in the Determination of Protein-Structure. *Crit. Rev. Biochem. Mol.* **1995**, *30*, 95−120.
(27) Arrondo, J. L. R.; Muga, A.; Castresana, J.; Goni, F. M. Quantitative Studies of the Structure of Proteins in Solution by Fourier-Transform Infrared-Spectroscopy. *Prog. Biophys. Mol. Biol.* **1993**, *59*, 23−56.
(28) Pelton, J. T.; McLean, L. R. Spectroscopic Methods for Analysis of Protein Secondary Structure. *Anal. Biochem.* **2000**, *277*, 167−176.
(29) Kong, J.; Yu, S. Fourier Transform Infrared Spectroscopic Analysis of Protein Secondary Structures. *Acta Biochim. Biophys. Sin.* **2007**, *39*, 549−559.
(30) Baugh, L.; Weidner, T.; Baio, J. E.; Nguyen, P. C. T.; Gamble, L. J.; Slayton, P. S.; Castner, D. G. Probing the Orientation of Surface-Immobilized Protein G B1 Using ToF-SIMS, Sum Frequency Generation, and NEXAFS Spectroscopy. *Langmuir* **2010**, *26*, 16434−16441.
(31) Weidner, T.; Apte, J. S.; Gamble, L. J.; Castner, D. G. Probing the Orientation and Conformation of α-Helix and β-Strand Model Peptides on Self-Assembled Monolayers Using Sum Frequency Generation and NEXAFS Spectroscopy. *Langmuir* **2010**, *26*, 3433−3440.
(32) Kim, J.; Somorjai, G. A. Molecular Packing of Lysozyme, Fibrinogen, and Bovine Serum Albumin on Hydrophilic and Hydrophobic Surfaces Studied by Infrared-Visible Sum Frequency Generation and Fluorescence Microscopy. *J. Am. Chem. Soc.* **2003**, *125*, 3150−3158.
(33) Liu, Y.; Jasensky, J.; Chen, Z. Molecular Interactions of Proteins and Peptides at Interfaces Studied by Sum Frequency Generation Vibrational Spectroscopy. *Langmuir* **2011**, *28*, 2113−2121.
(34) Mermut, O.; Phillips, D. C.; York, R. L.; McCrea, K. R.; Ward, R. S.; Somorjai, G. A. In Situ Adsorption Studies of a 14-Amino Acid Leucine-Lysine Peptide onto Hydrophobic Polystyrene and Hydrophilic Silica Surfaces Using Quartz Crystal Microbalance, Atomic Force Microscopy, and Sum Frequency Generation Vibrational Spectroscopy. *J. Am. Chem. Soc.* **2006**, *128*, 3598−3607.
(35) Wang, J.; Even, M. A.; Chen, X.; Schmaier, A. H.; Waite, J. H.; Chen, Z. Detection of Amide I Signals of Interfacial Proteins In Situ Using SFG. *J. Am. Chem. Soc.* **2003**, *125*, 9914−9915.
(36) Chen, X. Y.; Wang, J.; Boughton, A. P.; Kristalyn, C. B.; Chen, Z. Multiple Orientation of Melittin Inside a Single Lipid Bilayer Determined by Combined Vibrational Spectroscopic Studies. *J. Am. Chem. Soc.* **2007**, *129*, 1420−1427.
(37) Phillips, D. C.; York, R. L.; Mermut, O.; McCrea, K. R.; Ward, R. S.; Somorjai, G. A. Side Chain, Chain Length, and Sequence Effects on Amphiphilic Peptide Adsorption at Hydrophobic and Hydrophilic Surfaces Studied by Sum-Frequency Generation Vibrational Spectroscopy and Quartz Crystal Microbalance. *J. Phys. Chem. C* **2007**, *111*, 255−261.
(38) Weidner, T.; Breen, N. F.; Li, K.; Drobny, G. P.; Castner, D. G. Sum Frequency Generation and Solid-State NMR Study of the Structure, Orientation, and Dynamics of Polystyrene-Adsorbed Peptides. *Proc. Natl. Acad. Sci. U.S.A.* **2010**, *107*, 13288−13293.
(39) Ji, N.; Shen, Y. R. A Novel Spectroscopic Probe for Molecular Chirality. *Chirality* **2006**, *18*, 146−158.
(40) Ji, N.; Ostroverkhov, V.; Belkin, M.; Shiu, Y.-J.; Shen, Y.-R. Toward Chiral Sum-Frequency Spectroscopy. *J. Am. Chem. Soc.* **2006**, *128*, 8845−8848.
(41) Belkin, M.; Shen, Y. Non-Linear Optical Spectroscopy as a Novel Probe for Molecular Chirality. *Int. Rev. Phys. Chem.* **2005**, *24*, 257−299.
(42) Belkin, M.; Kulakov, T.; Ernst, K.; Yan, L.; Shen, Y. Sum-Frequency Vibrational Spectroscopy on Chiral Liquids: A Novel Technique to Probe Molecular Chirality. *Phys. Rev. Lett.* **2000**, *85*, 4474−4477.
(43) Simpson, G. J. Molecular Origins of the Remarkable Chiral Sensitivity of Second-Order Nonlinear Optics. *ChemPhysChem* **2004**, *5*, 1301−1310.
(44) Haupert, L. M.; Simpson, G. J. Chirality in Nonlinear Optics. *Annu. Rev. Phys. Chem.* **2009**, *60*, 345−365.
(45) Wang, H.-F.; Gan, W.; Lu, R.; Rao, Y.; Wu, B.-H. Quantitative Spectral and Orientational Analysis in Surface Sum Frequency Generation Vibrational Spectroscopy (SFG-VS). *Int. Rev. Phys. Chem.* **2005**, *24*, 191−256.
(46) Wang, J.; Chen, X.; Clarke, M. L.; Chen, Z. Detection of Chiral Sum Frequency Generation Vibrational Spectra of Proteins and Peptides at Interfaces In Situ. *Proc. Natl. Acad. Sci. U.S.A.* **2005**, *102*, 4978−4983.
(47) Walter, S. R.; Geiger, F. M. DNA on Stage: Showcasing Oligonucleotides at Surfaces and Interfaces with Second Harmonic and Vibrational Sum Frequency Generation. *J. Phys. Chem. Lett.* **2009**, *1*, 9−15.
(48) Stokes, G. Y.; Gibbs-Davis, J. M.; Boman, F. C.; Stepp, B. R.; Condie, A. G.; Nguyen, S. T.; Geiger, F. M. Making "Sense" of DNA. *J. Am. Chem. Soc.* **2007**, *129*, 7492−7493.
(49) Fu, L.; Liu, J.; Yan, E. C. Y. Chiral Sum Frequency Generation Spectroscopy for Characterizing Protein Secondary Structures at Interfaces. *J. Am. Chem. Soc.* **2011**, *133*, 8094−8097.
(50) Fu, L.; Ma, G.; Yan, E. C. Y. In situ Misfolding of Human Islet Amyloid Polypeptide at Interfaces Probed by Vibrational Sum Frequency Generation. *J. Am. Chem. Soc.* **2010**, *132*, 5405−5412.
(51) Fu, L.; Wang, Z.; Yan, E. C. Y. Chiral Vibrational Structures of Proteins at Interfaces Probed by Sum Frequency Generation Spectroscopy. *Int. J. Mol. Sci.* **2011**, *12*, 9404−9425.
(52) Fu, L.; Wang, Z.; Yan, E. C. Y. N-H Stretching Modes Around 3300 Wavenumber From Peptide Backbones Observed by Chiral Sum Frequency Generation Vibrational Spectroscopy. *Chirality* **2014**, *26*, 521−524.
(53) Fu, L.; Xiao, D.; Wang, Z.; Batista, V. S.; Yan, E. C. Y. Chiral Sum Frequency Generation for In Situ Probing Proton Exchange in Antiparallel β-sheets at Interfaces. *J. Am. Chem. Soc.* **2013**, *135*, 3592−3598.
(54) Xiao, D.; Fu, L.; Liu, J.; Batista, V. S.; Yan, E. C. Y. Amphiphilic Adsorption of Human Islet Amyloid Polypeptide Aggregates to Lipid/Aqueous Interfaces. *J. Mol. Biol.* **2012**, *421*, 537−547.
(55) Yan, E. C.; Fu, L.; Wang, Z.; Liu, W. Biological Macromolecules at Interfaces Probed by Chiral Vibrational Sum Frequency Generation Spectroscopy. *Chem. Rev.* **2014**, *114*, 8471−8498.
(56) Wang, Z.; Fu, L.; Yan, E. C. Y. C−H Stretch for Probing Kinetics of Self-Assembly into Macromolecular Chiral Structures at Interfaces by Chiral Sum Frequency Generation Spectroscopy. *Langmuir* **2013**, *29*, 4077−4083.
(57) Shen, Y. Surface Properties Probed by Second-Harmonic and Sum-Frequency Generation. *Nature* **1989**, *337*, 519−525.
(58) Eisenthal, K. Liquid Interfaces Probed by Second-Harmonic and Sum-Frequency Spectroscopy. *Chem. Rev.* **1996**, *96*, 1343−1360.
(59) Richmond, G. Molecular Bonding and Interactions at Aqueous Surfaces as Probed by Vibrational Sum Frequency Spectroscopy. *Chem. Rev.* **2002**, *102*, 2693−2724.
(60) Shen, Y.-R. *The Principles of Nonlinear Optics*; Wiley-Interscience: New York, 1984.
(61) Boyd, R. W. *Nonlinear Optics* Academic Press: San Diego, 2003.
(62) Lambert, A. G.; Davies, P. B.; Neivandt, D. J. Implementing the Theory of Sum Frequency Generation Vibrational Spectroscopy: A Tutorial Review. *Appl. Spectrosc. Rev.* **2005**, *40*, 103−145.
(63) Ma, G.; Liu, J.; Fu, L.; Yan, E. C. Y. Probing Water and Biomolecules at the Air−Water Interface with a Broad Bandwidth Vibrational Sum Frequency Generation Spectrometer from 3800 to 900 cm^{-1}. *Appl. Spectrosc.* **2009**, *63*, 528−537.
(64) Wang, J.; Clarke, M. L.; Chen, Z. Polarization Mapping: A Method to Improve Sum Frequency Generation Spectral Analysis. *Anal. Chem.* **2004**, *76*, 2159−2167.

DOI: 10.1021/jp508926e
J. Phys. Chem. B 2015, 119, 2769−2785

(65) Oh-e, M.; Yokoyama, H.; Yorozuya, S.; Akagi, K.; Belkin, M. A.; Shen, Y. R. Sum-Frequency Vibrational Spectroscopy of α Helically Structured Conjugated Polymer. *Phys. Rev. Lett.* **2004**, *93*, 267402.
(66) Fu, L.; Zhang, Y.; Wei, Z. H.; Wang, H. F. Intrinsic Chirality and Prochirality at Air/R-(+)- and S-(−)-Limonene Interfaces: Spectral Signatures With Interference Chiral Sum-Frequency Generation Vibrational Spectroscopy. *Chirality* **2014**, *26*, 509−520.
(67) Chiti, F.; Dobson, C. M. Protein Misfolding, Functional Amyloid, and Human Disease. *Annu. Rev. Biochem.* **2006**, *75*, 333−366.
(68) Braak, H.; Braak, E. Neuropathological Staging of Alzheimer-Related Changes. *Acta Neuropathol.* **1991**, *82*, 239−259.
(69) Hoppener, J. W. M.; Ahren, B.; Lips, C. J. M. Islet Amyloid and Type 2 Diabetes Mellitus. *N. Engl. J. Med.* **2000**, *343*, 411−419.
(70) Jayasinghe, S. A.; Langen, R. Membrane Interaction of Islet Amyloid Polypeptide. *Biochim. Biophys. Acta, Biomembr.* **2007**, *1768*, 2002−2009.
(71) Hebda, J. A.; Miranker, A. D. The Interplay of Catalysis and Toxicity by Amyloid Intermediates on Lipid Bilayers: Insights from Type II Diabetes. *Annu. Rev. Biophys.* **2009**, *38*, 125−152.
(72) Kayed, R.; Sokolov, Y.; Edmonds, B.; McIntire, T. M.; Milton, S. C.; Hall, J. E.; Glabe, C. G. Permeabilization of Lipid Bilayers Is a Common Conformation-Dependent Activity of Soluble Amyloid Oligomers in Protein Misfolding Diseases. *J. Biol. Chem.* **2004**, *279*, 46363−46366.
(73) Engel, M. F. M. Membrane Permeabilization by Islet Amyloid Polypeptide. *Chem. Phys. Lipids* **2009**, *160*, 1−10.
(74) Anguiano, M.; Nowak, R. J.; Lansbury, P. T. Protofibrillar Islet Amyloid Polypeptide Permeabilizes Synthetic Vesicles by a Pore-Like Mechanism That May Be Relevant to Type II Diabetes. *Biochemistry* **2002**, *41*, 11338−11343.
(75) Janson, J.; Ashley, R. H.; Harrison, D.; McIntyre, S.; Butler, P. C. The Mechanism of Islet Amyloid Polypeptide Toxicity is Membrane Disruption by Intermediate-Sized Toxic Amyloid Particles. *Diabetes* **1999**, *48*, 491−498.
(76) DeToma, A. S.; Salamekh, S.; Ramamoorthy, A.; Lim, M. H. Misfolded Proteins in Alzheimer's Disease and Type II Diabetes. *Chem. Soc. Rev.* **2012**, *41*, 608−621.
(77) Harrison, R. S.; Sharpe, P. C.; Singh, Y.; Fairlie, D. P. Amyloid Peptides and Proteins in Review. *Rev. Physiol. Biochem. Pharmacol.* **2007**, *159*, 1−77.
(78) Wilson, M. R.; Yerbury, J. J.; Poon, S. Potential Roles of Abundant Extracellular Chaperones in the Control of Amyloid Formation and Toxicity. *Mol. BioSyst.* **2008**, *4*, 42−52.
(79) Butterfield, S. M.; Lashuel, H. A. Amyloidogenic Protein Membrane Interactions: Mechanistic Insight from Model Systems. *Angew. Chem., Int. Ed.* **2010**, *49*, 5628−5654.
(80) Westermark, P.; Engstrom, U.; Johnson, K. H.; Westermark, G. T.; Betsholtz, C. Islet Amyloid Polypeptide-Pinpointing Amino-Acid-Residues Linked to Amyloid Fibril Formation. *Proc. Natl. Acad. Sci. U.S.A.* **1990**, *87*, 5036−5040.
(81) Degrado, W. F.; Lear, J. D. Induction of Peptide Conformation at Apolar Water Interfaces 0.1. A Study with Model Peptides of Defined Hydrophobic Periodicity. *J. Am. Chem. Soc.* **1985**, *107*, 7684−7689.
(82) An, M.; Wijesinghe, D.; Andreev, O. A.; Reshetnyak, Y. K.; Engelman, D. M. pH-(low)-Insertion-Peptide (pHLIP) Translocation of Membrane Impermeable Phalloidin Toxin Inhibits Cancer Cell Proliferation. *Proc. Natl. Acad. Sci. U.S.A.* **2010**, *107*, 20246−20250.
(83) Andreev, O. A.; Karabadzhak, A. G.; Weerakkody, D.; Andreev, G. O.; Engelman, D. M.; Reshetnyak, Y. K. pH (low) Insertion Peptide (pHLIP) Inserts across a Lipid Bilayer as a Helix and Exits by a Different Path. *Proc. Natl. Acad. Sci. U.S.A.* **2010**, *107*, 4081−4086.
(84) Palczewski, K.; Kumasaka, T.; Hori, T.; Behnke, C. A.; Motoshima, H.; Fox, B. A.; Le Trong, I.; Teller, D. C.; Okada, T.; Stenkamp, R. E.; et al. Crystal Structure of Rhodopsin: A G Protein-Coupled Receptor. *Science* **2000**, *289*, 739−745.
(85) Hebda, J. A.; Saraogi, I.; Magzoub, M.; Hamilton, A. D.; Miranker, A. D. A Peptidomimetic Approach to Targeting Pre-amyloidogenic States in Type II Diabetes. *Chem. Biol.* **2009**, *16*, 943−950.
(86) Palczewski, K. G. Protein-Coupled Receptor Rhodopsin. *Annu. Rev. Biochem.* **2006**, *75*, 743−767.
(87) Fox, R. O.; Richards, F. M. A Voltage-Gated Ion Channel Model Inferred from the Crystal-Structure of Alamethicin at 1.5-Å Resolution. *Nature* **1982**, *300*, 325−330.
(88) Salnikov, E. S.; Friedrich, H.; Li, X.; Bertani, P.; Reissmann, S.; Hertweck, C.; O'Neil, J. D. J.; Raap, J.; Bechinger, B. Structure and Alignment of the Membrane-Associated Peptaibols Ampullosporin A and Alamethicin by Oriented N-15 and P-31 Solid-State NMR Spectroscopy. *Biophys. J.* **2009**, *96*, 86−100.
(89) Matsuzaki, K.; Nakayama, M.; Fukui, M.; Otaka, A.; Funakoshi, S.; Fujii, N.; Bessho, K.; Miyajima, K. Role of Disulfide Linkages in Tachyplesin Lipid Interactions. *Biochemistry* **1993**, *32*, 11704−11710.
(90) Chen, X. Y.; Chen, Z. SFG Studies on Interactions between Antimicrobial Peptides and Supported Lipid Bilayers. *Biochim. Biophys. Acta, Biomembr.* **2006**, *1758*, 1257−1273.
(91) Laederach, A.; Andreotti, A. H.; Fulton, D. B. Solution and Micelle-bound Structures of Tachyplesin I and Its Active Aromatic Linear Derivatives. *Biochemistry* **2002**, *41*, 12359−12368.
(92) Jayasinghe, S. A.; Langen, R. Lipid Membranes Modulate the Structure of Islet Amyloid Polypeptide. *Biochemistry* **2005**, *44*, 12113−12119.
(93) Knight, J. D.; Hebda, J. A.; Miranker, A. D. Conserved and Cooperative Assembly of Membrane-Bound α-helical States of Islet Amyloid Polypeptide. *Biochemistry* **2006**, *45*, 9496−9508.
(94) Khemtemourian, L.; Engel, M. F. M.; Kruijtzer, J. A. W.; Hoppener, J. W. M.; Liskamp, R. M. J.; Killian, J. A. The Role of the Disulfide Bond in the Interaction of Islet Amyloid Polypeptide with Membranes. *Eur. Biophys. J.* **2010**, *39*, 1359−1364.
(95) Goldsbury, C.; Goldie, K.; Pellaud, J.; Seelig, J.; Frey, P.; Muller, S. A.; Kistler, J.; Cooper, G. J. S.; Aebi, U. Amyloid Fibril Formation from Full-Length and Fragments of Amylin. *J. Struct. Biol.* **2000**, *130*, 352−362.
(96) Brender, J. R.; Hartman, K.; Reid, K. R.; Kennedy, R. T.; Ramamoorthy, A. A Single Mutation in the Nonamyloidogenic Region of Islet Amyloid Polypeptide Greatly Reduces Toxicity. *Biochemistry* **2008**, *47*, 12680−12688.
(97) Englander, S. W. Protein Folding Intermediates and Pathways Studied by Hydrogen Exchange. *Annu. Rev. Biophys. Biomol. Struct.* **2000**, *29*, 213−238.
(98) Englander, S. W.; Downer, N. W.; Teitelba, H. Hydrogen Exchange. *Annu. Rev. Biochem.* **1972**, *41*, 903−924.
(99) Miranker, A.; Robinson, C. V.; Radford, S. E.; Aplin, R. T.; Dobson, C. M. Detection of Transient Protein-Folding Populations by Mass-Spectrometry. *Science* **1993**, *262*, 896−900.
(100) Schanda, P.; Brutscher, B. Very Fast Two-Dimensional NMR Spectroscopy for Real-Time Investigation of Dynamic Events in Proteins on the Time Scale of Seconds. *J. Am. Chem. Soc.* **2005**, *127*, 8014−8015.
(101) Mandell, J. G.; Falick, A. M.; Komives, E. A. Identification of Protein-Protein Interfaces by Decreased Amide Proton Solvent Accessibility. *Proc. Natl. Acad. Sci. U.S.A.* **1998**, *95*, 14705−14710.
(102) Garczarek, F.; Gerwert, K. Functional Waters in Intraprotein Proton Transfer Monitored by FTIR Difference Spectroscopy. *Nature* **2006**, *439*, 109−112.
(103) le Coutre, J.; Gerwert, K. Kinetic Isotope Effects Reveal an Ice-Like and a Liquid-Phase-Type Intramolecular Proton Transfer in Bacteriorhodopsin. *FEBS Lett.* **1996**, *398*, 333−336.
(104) Knight, J. D.; Miranker, A. D. Phospholipid Catalysis of Diabetic Amyloid Assembly. *J. Mol. Biol.* **2004**, *341*, 1175−1187.
(105) Conboy, J. C.; Messmer, M. C.; Richmond, G. L. Investigation of Surfactant Conformation and Order at the Liquid-Liquid Interface by Total Internal Reflection Sum-Frequency Vibrational Spectroscopy. *J. Phys. Chem.* **1996**, *100*, 7617−7622.
(106) Liljebad, J. F. D.; Bulone, V.; Rutland, M. W.; Johnson, C. M. Supported Phospholipid Monolayers. The Molecular Structure Investigated by Vibrational Sum Frequency Spectroscopy. *J. Phys. Chem. C* **2011**, *115*, 10617−10629.

DOI: 10.1021/jp508926e
J. Phys. Chem. B 2015, 119, 2769−2785

(107) Howell, N. K.; Arteaga, G.; Nakai, S.; Li-Chan, E. C. Y. Raman Spectral Analysis in the C-H Stretching Region of Proteins and Amino Acids for Investigation of Hydrophobic Interactions. *J. Agric. Food Chem.* **1999**, *47*, 924−933.
(108) Toth, S. J.; Madden, J. T.; Taylor, L. S.; Marsac, P.; Simpson, G. J. Selective Imaging of Active Pharmaceutical Ingredients in Powdered Blends with Common Excipients Utilizing Two-Photon Excited Ultraviolet-Fluorescence and Ultraviolet-Second Order Nonlinear Optical Imaging of Chiral Crystals. *Anal. Chem.* **2012**, *84*, 5869−5875.
(109) Yan, E. C. Y.; Kazmi, M. A.; Ganim, Z.; Hou, J. M.; Pan, D. H.; Chang, B. S. W.; Sakmar, T. P.; Mathies, R. A. Retinal Counterion Switch in the Photoactivation of the G protein-Coupled Receptor Rhodopsin. *Proc. Natl. Acad. Sci. U.S.A.* **2003**, *100*, 9262−9267.
(110) Lewis, A.; Spoonhow, J.; Bogomoln, Ra; Lozier, R. H.; Stoecken, W. Tunable Laser Resonance Raman-Spectroscopy of Bacteriorhodopsin. *Proc. Natl. Acad. Sci. U.S.A.* **1974**, *71*, 4462−4466.
(111) Yan, E. C. Y.; Ganim, Z.; Kazmi, M. A.; Chang, B. S. W.; Sakmar, T. P.; Mathies, R. A. Resonance Raman Analysis of the Mechanism of Energy Storage and Chromophore Distortion in the Primary Visual Photoproduct. *Biochemistry* **2004**, *43*, 10867−10876.
(112) Surewicz, W. K.; Mantsch, H. H. New Insight into Protein Secondary Structure from Resolution-Enhanced Infrared-Spectra. *Biochim. Biophys. Acta* **1988**, *952*, 115−130.
(113) Friedrich, T.; Geibel, S.; Kalmbach, R.; Chizhov, I.; Ataka, K.; Heberle, J.; Engelhard, M.; Bamberg, E. Proteorhodopsin is a Light-Driven Proton Pump with Variable Vectoriality. *J. Mol. Biol.* **2002**, *321*, 821−838.
(114) Yan, E. C. Y.; Epps, J.; Lewis, J. W.; Szundi, I.; Bhagat, A.; Sakmar, T. P.; Kliger, D. S. Photointermediates of the Rhodopsin S186A Mutant as a Probe of the Hydrogen-Bond Network in the Chromophore Pocket and the Mechanism of Counterion Switch. *J. Phys. Chem. C* **2007**, *111*, 8843−8848.
(115) Mooney, V. L.; Szundi, I.; Lewis, J. W.; Yan, E. C. Y.; Kliger, D. S. Schiff Base Protonation Changes in Siberian Hamster Ultraviolet Cone Pigment Photointermediates. *Biochemistry* **2012**, *51*, 2630−2637.
(116) Perry, J. M.; Moad, A. J.; Begue, N. J.; Wampler, R. D.; Simpson, G. J. Electronic and Vibrational Second-Order Nonlinear Optical Properties of Protein Secondary Structural Motifs. *J. Phys. Chem. B* **2005**, *109*, 20009−20026.
(117) Nguyen, K. T.; King, J. T.; Chen, Z. Orientation Determination of Interfacial β-Sheet Structures In Situ. *J. Phys. Chem. B* **2010**, *114*, 8291−8300.
(118) Nguyen, K. T.; Le Clair, S. V.; Ye, S. J.; Chen, Z. Orientation Determination of Protein Helical Secondary Structures Using Linear and Nonlinear Vibrational Spectroscopy. *J. Phys. Chem. B* **2009**, *113*, 12169−12180.

DOI: 10.1021/jp508926e
J. Phys. Chem. B 2015, 119, 2769−2785